Hadron multiplicity fluctuations in perturbative QCD[†]

Yu.L. Dokshitzer*
Riga Technical University, Latvia

B.R. Webber
Cavendish Laboratory, University of Cambridge, UK

Abstract

We examine hadron multiplicity fluctuations in hard processes and confront analytic QCD predictions with the pattern of multiplicity fluctuations observed in e^+e^- annihilation and high-p_t jets produced in pp collisions at the LHC. Special emphasis is placed on high-multiplicity fluctuations in jets. Selecting events with hadronic multiplicity exceeding the average value by a factor of 3 or more in various processes has been a source of conundrums for many years. We discuss two recent high-multiplicity puzzles and attempt to reveal their common origin.

[†] We dedicate this paper to the memory of our late collaborator and friend Pino Marchesini, in the hope that he would have found it sufficiently amusing and provocative.

* on leave from St Petersburg Nuclear Physics Institute, Russia

Contents

1   Introduction

> 'Begin at the beginning and go on till you come to the end: then stop' [1]

A consistent QCD description of the pattern of multiplicity fluctuations in hard processes is lacking. In this paper, we extend an improved perturbative QCD analysis of multiplicity fluctuations in a gluon jet [2] to arbitrary ensembles of jets with a commensurate hardness scale, such as e^+e^- annihilation into hadrons (viewed as 2 quark jets), hadronic Higgs or Υ decay (2 or 3 gluon jets), multiplicity distribution in one hemisphere of e^+e^- annihilation and in high-p_t LHC jet studies (one quark or, one day, one gluon), *etc.*

In terms of QCD predictions being compared with experiment, we do not aim at fitting the data optimally. Instead, we demonstrate that the QCD dynamics of parton multiplication is compatible with observation and provides reasonable quantitative agreement.

In Section 2 necessary theoretical formulae are presented.

Section 3 is devoted to phenomenology.

In Section 4 we discuss two strange phenomena in high-multiplicity fluctuations that may have a common origin, namely an unexpected flattening of the high-multiplicity tail of ATLAS jets [4] and an amusing behaviour of long-range ellipticity recently observed by CMS [3].

2   Multiplicity fluctuations

> 'It would be so nice if something made sense for a change' [1]

2.1   Polyakov − KNO

In 1970 A.M. Polyakov [5] considered multiparticle production in e^+e^- annihilation in the framework of an abstract QFT. By assuming *scale similarity* of microscopic dynamics he arrived at what we know now as KNO scaling [6]:

$$P_n(Q) \equiv \frac{\sigma_n}{\sigma_{\text{tot}}} = [N(Q)]^{-1}\Psi(\nu), \quad \nu \equiv \frac{n}{N(Q)}, \tag{2.1a}$$

with $N(Q)$ the mean particle multiplicity

$$N(Q) = \sum_{n=1}^{\infty} nP_n(Q) \equiv \langle n \rangle(Q). \tag{2.1b}$$

In the QCD framework, the validity of the asymptotic scaling regime (2.1) was envisaged by Basetto, Ciafaloni and Marchesini as a consequence of the cascading nature of parton multiplication in [7]. An analytic solution of the scaling distribution in the limit $\alpha_s \to 0$ was obtained later in [8] (see [9] for a review).

Polyakov arrived at the scaling law by employing the general properties of unitarity and dispersion relations. More than that: he also predicted that the probability of high-multiplicity fluctuations should fall at $\nu \gg 1$ faster than exponentially, namely as

$$\Psi(\nu) \propto e^{-\nu^\mu}, \qquad \mu = \frac{1}{1-\gamma}, \tag{2.2a}$$

where the exponent μ is related to the anomalous dimension of mean multiplicity energy growth

$$\gamma \equiv \frac{d}{\ln Q} \ln N(Q). \tag{2.2b}$$

Polyakov's amusing prediction remained virtually unnoticed. And understandably so: back in 1970 hardly anyone believed in the possibility of applying QFT dynamics to the physics of hadrons.

In Polyakov's scale-invariant model γ was constant. In QCD, scale invariance is broken by the running of the coupling, and $\gamma = \gamma(\alpha_s(Q))$ implying logarithmic scaling violation.

Hadron–hadron interactions fall into two categories: large-cross-section, limited-transverse-momenta phenomena (total, diffractive, minimum bias inelastic "soft" processes) and small-cross-section, large-transverse-momenta "hard" collisions.

The physics of the two is essentially different. In particular, the validity of phenomenological KNO scaling in hadron–hadron interactions was always a mystery. The tension has only recently eased when it became clear that the KNO scaling vanishes with increasing collision energy.

In hard interactions, the situation is directly opposite. Here, the scaling law (2.1) *has to hold*, at least at a sufficiently large hardness scale Q.

In order to stress the difference, and in tribute to Polyakov's precocious discovery, we will hereafter refer to the multiplicity pattern (2.1) *in hard processes* as **P-KNO scaling**.

2.2   DLA

The asymptotic P-KNO function [8] was derived in perturbative QCD in the leading double-logarithmic approximation (DLA). The normalized factorial moments of the multiplicity distribution

$$g_k(Q) \equiv \frac{\langle n(n-1)\cdots(n-k+1)\rangle\,(Q)}{[N(Q)]^k} = \int_0^\infty d\nu\,\nu^k\,\Psi(\nu,Q) \tag{2.3}$$

satisfy a recurrence relation following from the evolution equation for cascading multiplication of gluons and can be calculated recursively. In the $Q \to \infty$ limit ($\alpha_s(Q) \to 0$) they cease to depend on the hardness scale Q, thus satisfying P-KNO scaling. For large rank k the moments can be found analytically,

$$g_k^{\mathrm{DLA}} \simeq \frac{2k!}{C^k}\left(k + \frac{1}{3k}\right) \qquad (k \gg 1). \tag{2.4a}$$

Here C is a number determined by the equation [8,9]

$$\ln C = \int_1^\infty \frac{dx}{x}\left(\frac{1}{\sqrt{2(x-1-\ln x)}} - \frac{1}{x-1}\right) \simeq 0.937, \quad C \simeq 2.552. \tag{2.4b}$$

Properly processed, (2.4) results in exponential falloff of the P-KNO distribution

$$\Psi(\nu) \simeq 2C\left(C\nu - 1 + \frac{1}{3C\nu}\right)\cdot e^{-C\nu}, \quad \nu \gg 1. \tag{2.5}$$

The accuracy of (2.4) and of the corresponding expression for the tail (2.5) was estimated in [8] as

$$\left[1 + \mathcal{O}\!\left(\frac{\ln(C\nu)}{(C\nu)^4}\right)\right]. \tag{2.6}$$

Surprisingly, the asymptotic formula for multiplicity moments (2.4) also proves to agree quite well with the exact values of low rank moments (see Appendix A).

The DLA solution proved to be too broad and fatally unrealistic. QCD corrections to the multiplicity moments were found to be "*so large that terms of yet higher order are unlikely to be negligible*" [10].

In next-to-leading order, the lowest few moments were found to be similar to those of a negative binomial distribution [11].

2.3   Improved QCD treatment of the P-KNO phenomenon (MDLA)

Observables that are driven by soft-gluon multiplication have perturbative series running in powers of the multiplicity anomalous dimension $\gamma = \mathcal{O}\!\left(\sqrt{\alpha_s}\right)$.

In [12] the observation was made that specific *next-to-next-to-leading order* terms of the series in $\sqrt{\alpha_s}$ *explode*: their magnitude increases linearly with the rank k of the multiplicity moment.

Expressed in terms of γ, the perturbative expansion for the moments of the P-KNO distribution g_k can be cast as

$$g_k = g_k^{\left[\mathrm{DLA}\right]} + g_k^{\left[\mathrm{MLLA}\right]} \cdot \gamma(\alpha_s) + g_k^{\left[\mathrm{NMLLA}\right]} \cdot \gamma^2(\alpha_s) + \dots \tag{2.7}$$

The *second* subleading term in this series possesses an explosive piece,

$$g_k^{\left[\mathrm{NMLLA}\right]} = g_k^{\left[\mathrm{DLA}\right]} \left[c\,k^2 + \mathcal{O}(k)\right]. \tag{2.8}$$

Such "explosiveness" systematically reproduces itself at higher orders in γ in the form of a series in $k\gamma$.

In [2] the origin of such corrections was understood to be due to energy conservation in parton cascading, which is deliberately ignored in the DLA. A simplified theoretical model was constructed that permitted one to single out these specific contributions and resum them to all orders in $k\gamma$ for a gluon jet.

This approximation one might label as the *Modified Double Log Approximation* (MDLA) in analogy with MLLA — the Modified Leading Log Approximation of [13,14,9].

In this paper, we generalise MDLA to the case of a quark jet or an arbitrary jet ensemble and confront the resulting theoretical formulae with experiment.

In the MDLA treatment, high-rank multiplicity moments $k \gg 1$ acquire a multiplier

$$g_k \simeq g_k^{\mathrm{DLA}} \cdot \frac{[\Gamma(1+\gamma)]^k}{\Gamma(1+k\gamma)} = \frac{2}{\tilde{C}^k}\left(k + \frac{1}{3k}\right) \cdot \cdot \frac{\Gamma(1+k)}{\Gamma(1+k\gamma)}, \qquad \tilde{C} \equiv \frac{C}{\Gamma(1+\gamma)}. \tag{2.9}$$

MDLA is likely to have imperfections. In particular, expansion of the MDLA factor in (2.9) produces powers of π that are not apparent in the exact NNLO calculation of the low-rank multiplicity moments [15]. Nevertheless, we consider it trustworthy in that it takes proper care of an important part of the physics of parton cascades: the energy balance.

The ratio of Γ-functions is analysed in Appendix B. Introducing

$$D \equiv \tilde{C}\,\gamma^\gamma(1-\gamma)^{1-\gamma} = C\frac{\gamma^\gamma(1-\gamma)^{1-\gamma}}{\Gamma(1+\gamma)}, \tag{2.10}$$

it can be cast in the form

$$g_k = \frac{2}{D^k}\left(k + \frac{1}{3k}\right)\Gamma(1 + k(1-\gamma)) \cdot \chi(k). \tag{2.11a}$$

The factor χ in (2.11a) can be approximated as (see Appendix B)

$$\chi(k) \approx \sqrt{\frac{1+k}{2\pi(1+\gamma k)(1+(1-\gamma)k)}} \cdot e\left(1 + \frac{1}{\gamma k}\right)^{-\gamma k}. \tag{2.11b}$$

From (2.11b) it is clear that $\chi(k)$ contains no factorial nor exponential growth with k. It starts from $\chi(0) \approx 1$ and gradually decreases as $1/\sqrt{k}$ when $k \to \infty$.

An alternative to (2.11) covers factorials, exponents *and* powers of k:

$$g_k = \frac{2}{D^k}\left(k + \frac{1}{3k}\right)\Gamma(\tfrac{1}{2} + (1-\gamma)k) \cdot \mathcal{F}(k). \tag{2.12a}$$

Here $\mathcal{F}$ is another slowly varying prefactor analogous to χ (2.11b). Approximately, (see Appendix C for a more accurate formula)

$$\mathcal{F}(k,\gamma) \simeq \frac{1}{\sqrt{2\pi}}\sqrt{\frac{1+k}{1+\gamma k}}. \tag{2.12b}$$

4

This one starts off from $(2\pi)^{-\frac{1}{2}}$ and freezes when $\gamma k \gg 1$. The transition between the two regimes for each prefactor is governed by the value of the product γk. It is that very key parameter that formed the basis for the MDLA approach.

The two approximations are identical at large k and serve different purposes.

The first is better suited for analysis of the interval of moment ranks $\gamma k < 1$ and, in particular, for verification of the formal asymptotic limit $\gamma \to 0$ (which we hereafter refer to as the DLA limit).

Given that γ in reality is not so small, the second form (2.12) is more practical.

The moments (2.11a), (2.12a) are characteristic of a *generalised Gamma distribution* and result in the following expression for the P-KNO tail (see Appendix C for the derivation).

$$\Psi(\nu) = \frac{2\mu^2}{\nu} \left([D\nu]^{2\mu} - [D\nu]^{\mu} + \frac{1}{3\mu^2} \right) e^{-[D\nu]^{\mu}} \cdot \chi(k_{\rm sd}); \tag{2.13a}$$

$$\Psi(\nu) = \frac{2\mu^2}{\nu} \left([D\nu]^{\frac{3}{2}\mu} - \frac{1}{2}[D\nu]^{\frac{1}{2}\mu} + \frac{1}{3\mu}[D\nu]^{-\frac{1}{2}\mu} \right) \cdot \mathcal{F}(k_{\rm sd}). \tag{2.13b}$$

In the limit $\gamma \to 0$ we have $\mu = 1$, $D = C$, $k_{\rm sd} = C\nu - 2$, $\chi(k) = 1$, and (2.13a) turns into the asymptotic DLA expression (2.5).

In the course of reconstruction of the distribution $\Psi(\nu)$ from its moments, we evaluate the prefactors $\chi(k)$, $\mathcal{F}$ at a characteristic point $k = k_{\rm sd}(\nu)$.
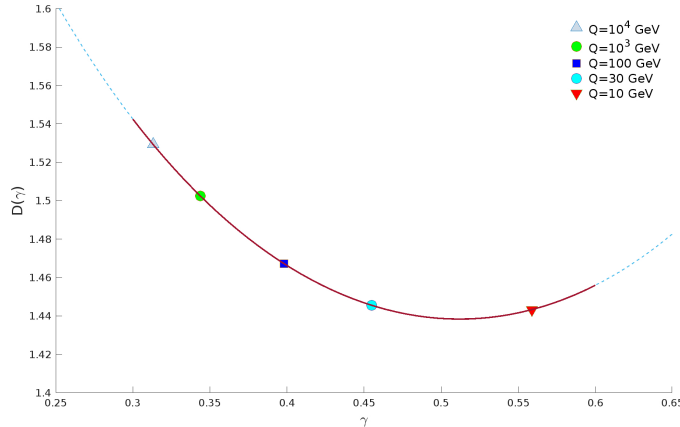

Figure 1: $D(\gamma)$ with typical hardness scales marked

The characteristic rank of multiplicity correlators $k_{\rm sd}(\nu)$ that corresponds to a given multiplicity ratio ν in a gluon jet is derived in Appendix C with $1/k^2$ accuracy.

It reads

$$k_{\rm sd}(\nu) \equiv \mu\left([D(\gamma)\nu]^{\mu} - 2\left[\tfrac{3}{2}\right]\right). \tag{2.14}$$

The different numbers to be subtracted depend on the choice between Eqs. (2.13a) and (2.13b), respectively.

Fig. 1 displays the function $D(\gamma)$ defined by (2.10). It shows that on realistic hardness scales D stays near 1.5.

It is important to stress that the scale dependence of the perturbative QCD P-KNO distribution is contained in a single quantity, that is, the multiplicity anomalous dimension $\gamma(\alpha_s(Q))$.

2.4 Multiplicity anomalous dimension

There are different ways to determine the value and the momentum dependence of γ. For example, one could read it directly from the data on the mean multiplicity of hadron in e^+e^- annihilation. We chose a more "theoretical" approach: to use the two-loop QCD expression [16]

$$\gamma(\alpha_s) = \sqrt{2N_c \frac{\alpha_s}{\pi}} - \left(\frac{\beta_0}{4} + \frac{10n_f}{3N_c^2}\right)\frac{\alpha_s}{2\pi}, \quad \beta_0 = \frac{11}{3}N_c - \frac{2}{3}n_f. \tag{2.15}$$

The coupling constant here refers to the "physical" coupling scheme also known as "bremsstrahlung" or CMW scheme [17], see also [18] and references therein.

In order to make our endeavour more challenging and in the hope of being more convincing, we chose not to play with the value of α_s.

We accept the world average

$$\alpha_{\overline{\text{MS}}}(M_Z) = 0.119$$

which translates into

$$\alpha_s(M_Z) \simeq 0.127$$

for the CMW coupling ($n_f = 5$).

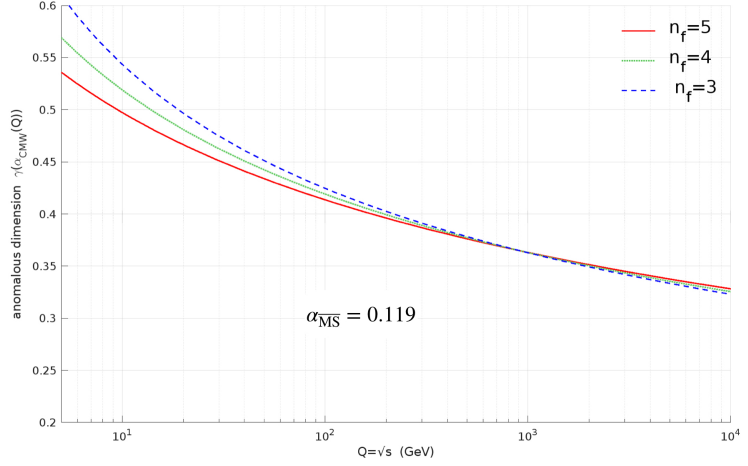Details of our coupling model are discussed in Appendix D.

Figure 2: Anomalous dimension of mean multiplicity

Experimental information on multiplicity fluctuations inside identified *gluon* jets is quite poor. In order to apply MDLA wisdom to the data we first need to generalise (2.13) to describe a quark jet, 2-quark systems (e^+e^-), etc.

2.5 Quark jet and multi-jet ensembles

To compute the P-KNO distribution for emission from an assembly of m_q quarks and/or antiquarks and m_g gluons, with comparable hardness, from that of a single hard gluon, (2.11), one must introduce a "source strength" parameter

$$\rho = m_q \rho_q + m_g \tag{2.16}$$

where ρ_q is the mean multiplicity for a quark jet, relative to that of a gluon jet.

The derivation of $\Psi^{(\rho)}$ for $\rho \neq 1$ then goes through three steps:

1. Laplace transform the gluon P-KNO function (2.13) onto the complex β-plane

$$\Phi(\beta) = \int_0^\infty d\nu\, \Psi(\nu)\, e^{-\beta\nu}. \tag{2.17a}$$

2. Construct the Laplace image

$$\Phi^{(\rho)}(\beta) \simeq \left[\Phi\left(\frac{\beta}{\rho}\right)\right]^\rho. \tag{2.17b}$$

3. Evaluate the inverse Laplace transform

$$\Psi^{(\rho)}(\nu) = \int_{\mathcal{C}} \frac{d\beta}{2\pi i}\, \Phi^{(\rho)}(\beta)\, e^{\beta\nu}. \tag{2.17c}$$

As far as the tail of the multiplicity distribution is concerned, *i.e.* for 'large' ν, the first and third steps (2.17a) and (2.17c) can be carried out with the help of the steepest descent and stationary phase methods, see Appendix C for details.

The final result reads

$$\Psi^{(\rho)}(\nu) = \sqrt{\rho}\, \frac{\mu^2}{\nu} \left[\nu\Psi(\nu)\right]^\rho \cdot \left(\frac{2\sqrt{2\pi}}{\sqrt{\gamma[D\nu]^\mu + 2\left[\frac{3}{2}\right](1-\gamma)}}\right)^{\rho-1}. \tag{2.18}$$

When $\rho = 1$ this expression coincides with the original *gluon jet* distribution (2.13).

For $\nu\Psi$ in the square brackets one can substitute either of representations (2.11), (2.12), with the corresponding change in the denominator.

In practice, we shall use the latter and compare with data in the range $\nu > 1$.

3 P-KNO phenomenology

Now that we have all the necessary formulas prepared, we can begin to test them phenomenologically. The bulk of high-quality data on multiplicity fluctuations come from e^+e^- annihilation.

3.1 Quark jet vs. Gluon jet

One routinely identifies the e^+e^- annihilation final state with a $q\bar{q}$ ensemble.
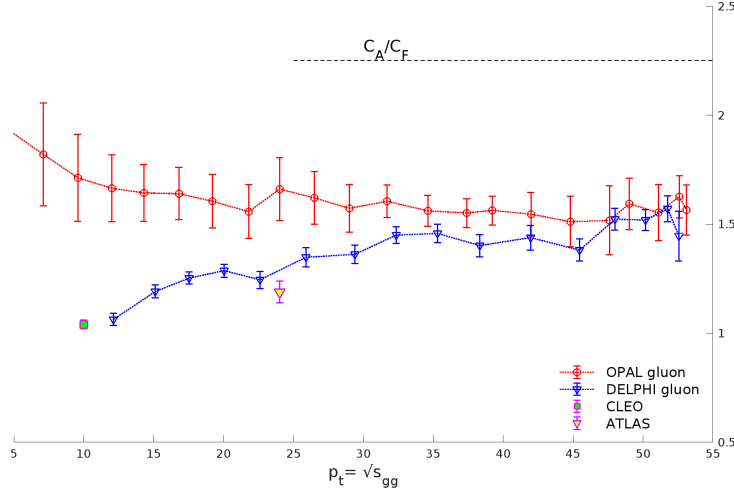
Figure 3: Ratio of charged hadron multiplicities in g- and q-initiated jets, [19–22]

This is a reasonable thing to do with a few percent accuracy.

Within this logic, the parameter ρ should be fixed in (2.18) as $\rho = 2\rho_q$. For gluon emission one would expect asymptotically

$$\rho_q = \frac{C_F}{C_A} = \frac{4}{9}.$$

However, for charged hadron emission at present energies the gluon-to-quark multiplicity ratio stays stubbornly close to 1.5; see Fig. 3.

Therefore for phenomenology we adopt the value $\rho_q = 2/3$.

3.2 Sensitivity to ρ and scaling violation

Fig. 4 demonstrates the sensitivity of the distribution (2.18) to the value of ρ and to the jet hardness scale.
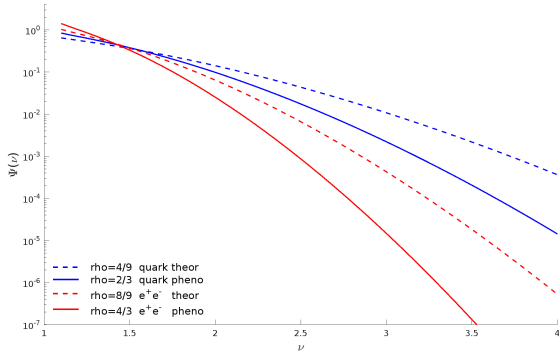
Figure 4a: Quark jet variation with ρ.
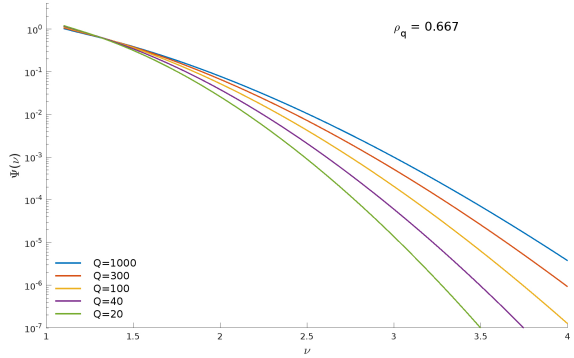
Figure 4b: Gluon jet variation with hardness Q.

3.3 P-KNO e^+e^- tail

In Fig. 5 we compare experimental data from e^+e^- annihilation [23,24] with theoretical curves corresponding to the two prescriptions for the P-KNO distribution, (2.11), (2.12), with $\rho = 2\rho_q = 4/3$. Both give a good description of the tail, with the latter extending even somewhat below $\nu = 1$.

7

Figure 5: Multiplicity fluctuations in e^+e^- annihilation: two theoretical expressions

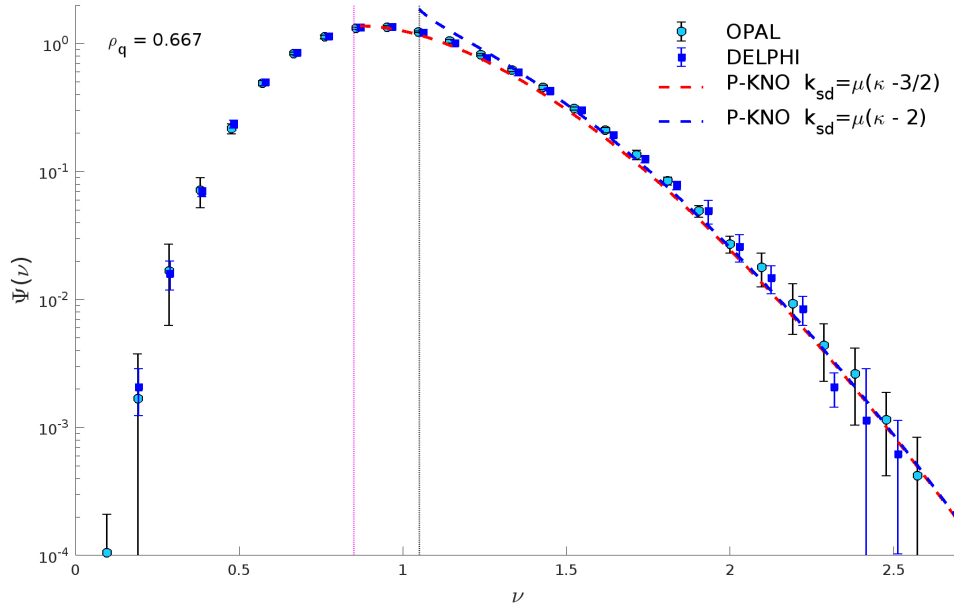In Fig. 6 we compare theoretical curves corresponding to two prescriptions for the parameter ρ. This shows what happens when we substitute the phenomenologically motivated $\rho_q = \frac{2}{3}$ ratio for the ρ parameter in (2.18). Now, the QCD curve agrees significantly better with the data.

3.4 Scaling violation (?)

Being an optimist, one could even see a hint of perturbatively controlled *scaling violation* by comparing the P-KNO tails of the TASSO (44 GeV) [25] and OPAL [23] and DELPHI (91 GeV) distributions [24] shown in Fig. 7.

3.5 ATLAS jets

The transverse momenta of the high-p_t jets studied by ATLAS at the LHC at $\sqrt{s} = 13$ TeV span a wide range of p_t, from 0.1 to 2.5 TeV [4]. Among other things, the multiplicity distributions of charged hadrons were reported. Translated into the P-KNO form, as shown in Fig. 8, the tails of these distributions are well matched by the QCD formula (2.18). We stress that this "fit" does not contain any fitting parameter. The only input is the value of $\rho = \frac{2}{3}$ since we treat such high-p_t jets as quark-originated.

Fig. 9 shows how the P-KNO curves change when one changes ρ from a theoretical quark value of $\frac{4}{9}$ to the value motivated by e^+e^- phenomenology, $\rho = \rho_q \simeq \frac{2}{3}$, as used in Fig. 8, which again does the best job.

There is a hint in [4] that the lower p_t intervals might contain a significant portion of gluon-initiated jets. However, it seems to us premature to dive into this potentially interesting issue. The available data on the multiplicity distribution in gluon jets is as yet insufficient.

3.6 Jet hardness

Meanwhile one subtle point should be mentioned here. There is a problem of how to determine the hardness scale for a jet stemming from a hadron–hadron collision. This is not as straightforward as for e^+e^- annihilation.

Hardness is a parameter that measures the state of development of the parton cascade and eventually the multiplicity of final hadrons.

In terms of quantum physics, one cannot state that a given particle *belongs* to a given jet. We some-what arbitrarily assemble the jets by *assigning* particles to them. In doing so we follow the QFT-dictated
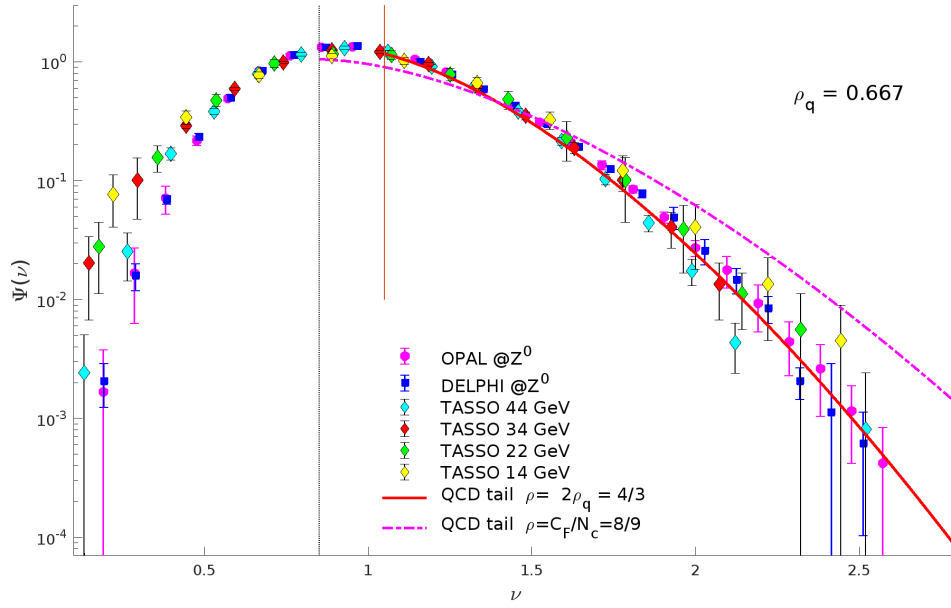
Figure 6: Multiplicity fluctuations in e^+e^- annihilation: checking ρ_q
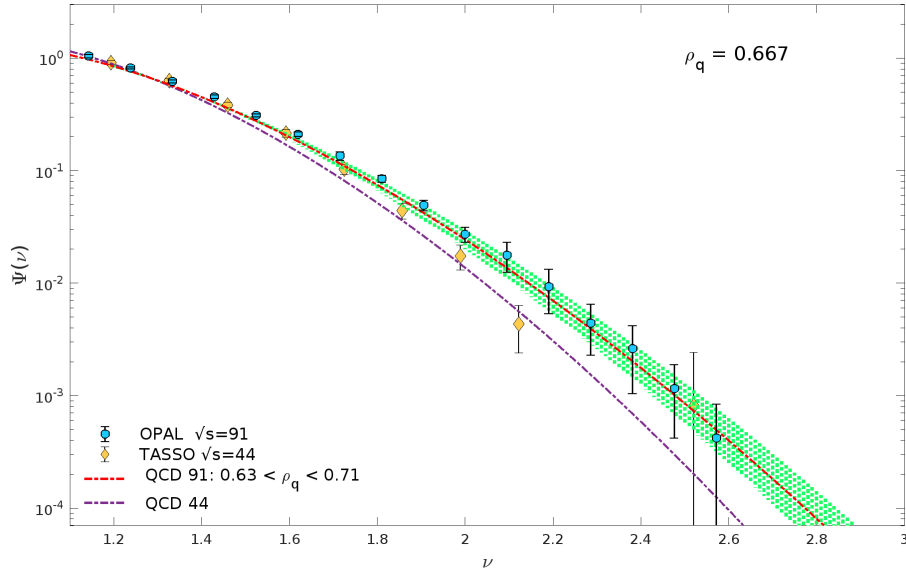
Figure 7: Hint at scaling violation in the P-KNO tail

pattern of collinear enhancements. The property of Angular Ordering in time-like parton cascades allows one to embody the total yield of final particles into a sum of a small number of jets with definite (individual geometry-dependent) hardness.

For an individual jet, the hardness parameter is determined by *the maximal transverse momentum* of particles assigned to this jet:

$$P_{t,\max} = 2E_{\text{jet}} \sin \frac{\Theta}{2}. \tag{3.1}$$

Here E_{jet} is the energy of the jet and Θ its opening angle. This definition implies that studying the jet content (particle energy spectra, multiplicity, etc.) one has count only particles that fit inside a given angular cone.
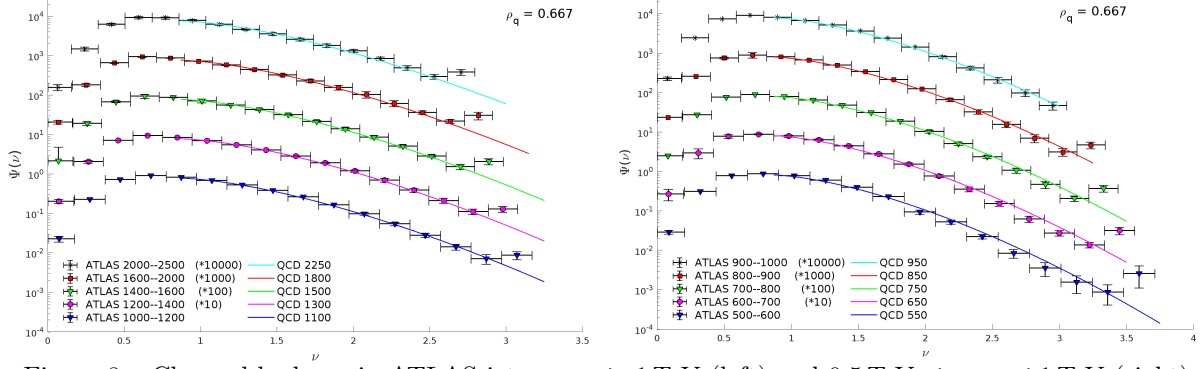
Figure 8: Charged hadrons in ATLAS jets: $p_{t,\text{jet}} \geq 1\,\text{TeV}$ (left) and $0.5\,\text{TeV} \leq p_{t,\text{jet}} \leq 1\,\text{TeV}$ (right)
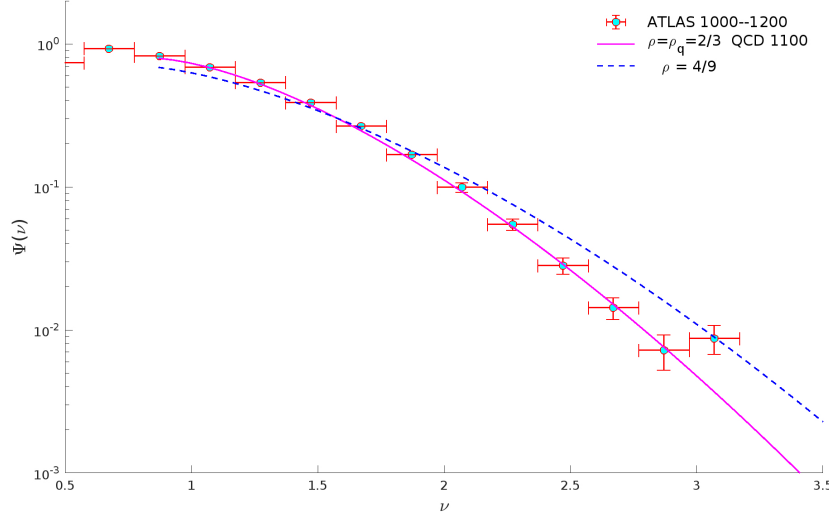
Figure 9: On sensitivity to ρ

For example, in $e^+e^- \to q\bar{q}$ one sets in (3.1) the opening angle $\Theta = \pi$ for each of the two jets to obtain

$$N_{e^+e^-} = 2\,n_q(P_{t,\max}^2 = s). \tag{3.2}$$

This means one treats the multiplicity of e^+e^- annihilation events as the sum of two independent quark jets. In so doing, hard-collinear as well as soft-large-angle emissions are taken care of, which contribute at the level of $\mathcal{O}(\gamma) \propto \sqrt{\alpha_s}$ relative to the leading DLA answer. The next-to-next-to leading correction $\mathcal{O}(\gamma^2) \propto \alpha_s$ would come from large-angle hard-gluon radiation (3 jets) and from correlated large-angle radiation of two energy-ordered soft gluons.

For 3-jet e^+e^- annihilation events, the full secondary particle multiplicity (including soft large-angle radiation) can be cast as [26]

$$N_{e^+e^-\to q\bar{q}g}(s) = N_{e^+e^-\to q\bar{q}}(s_{q\bar{q}}) + \tfrac{1}{2}N_{gg}(K_t^2), \quad s_{q\bar{q}} = 2(p_q p_{\bar{q}}), \quad K_t^2 \equiv \frac{2(p_g p_q)(p_g p_{\bar{q}})}{(p_q p_{\bar{q}})}, \tag{3.3}$$

where N_{gg} stands for the multiplicity in an event of two-gluon production by a colourless source, and K_t is the transverse momentum of the gluon in the $q\bar{q}$ center of mass frame.

Eq. (3.3) was tested experimentally and resulted in a measurement of the QCD C_F/C_A ratio [19].

To produce the P-KNO curves in Fig. 8 we chose the hardness scale as

$$Q = 2\,\overline{P_t}\,\sin\frac{R}{2}, \quad R = 0.4, \tag{3.4}$$

with $\overline{P_t}$ the middle point of the p_t interval and R the "angular radius" parameter of the anti-kt jet finder employed by ATLAS. Varying the scale in (3.4) by a factor of 2 or more has a negligible effect on the predicted P-KNO distribution, because at such large p_t $\gamma(\alpha_s(Q))$ varies very little.

3.7 One hemisphere

A hard test is provided by the DELPHI measurement of multiplicity fluctuations in a single quark jet (one hemisphere of e^+e^- annihilation) [24]. Here, instead of $\rho = 2\rho_q = \frac{4}{3}$, we have to use $\rho = \rho_q = \frac{2}{3}$. The result is displayed in Fig. 10.

The dashed line sets the applicability limit of (2.12). Below $\nu \approx 0.85$ the formula breaks when k_{sd} becomes negative. With representation (2.11) this happens even earlier, at $\nu \approx 1.05$.

We do not have a solid explanation for why a "tail formula" permits extension all the way down to the peak of the P-KNO spectrum.
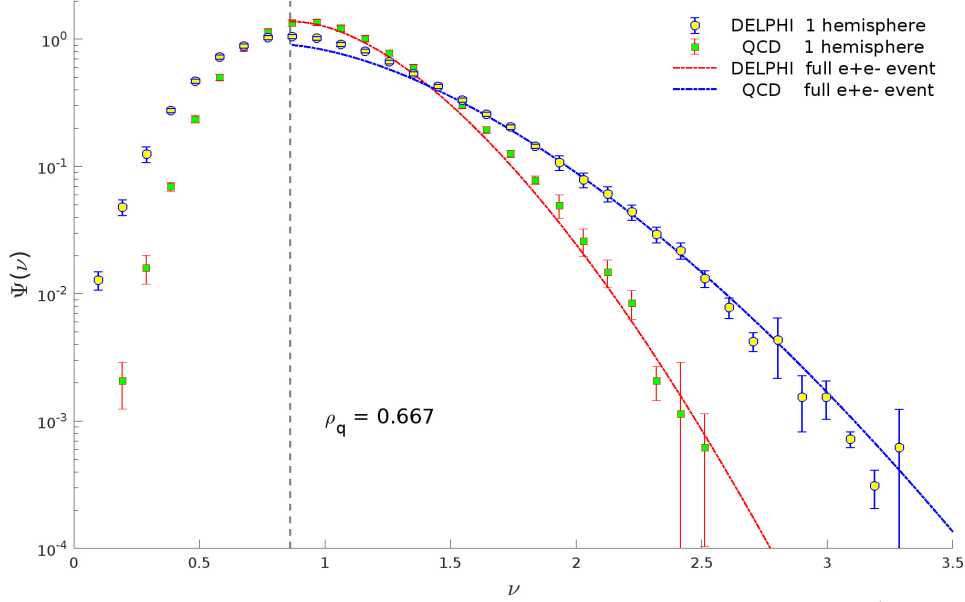
Figure 10: Comparison of multiplicity fluctuations in one hemisphere with full e^+e^- event [24].

The agreement is not perfect, but still impressive given that there are no tuning parameters involved.

There is an interesting point here in relation to the hardness scale.

Measurement in one hemisphere means that the maximum allowed radiation angle equals $\frac{\pi}{2}$. According to (3.1), this implies the hardness scale

$$Q_1 = 2E_{\mathrm{jet}} \sin \frac{\Theta}{2} = 2E_{\mathrm{jet}} \sin \frac{\pi}{4} = \sqrt{s} \cdot \frac{1}{\sqrt{2}}. \tag{3.5}$$

For full e^+e^- annihilation events we have $Q = \sqrt{s}$ ($\Theta = \pi$). This may seem confusing: e^+e^- annihilation is a sum of two hemispheres, is it not? It is when it concerns mean multiplicity but not so for multiplicity correlators!

A quark radiates in all directions, producing the bulk of offspring

$$N_{own} = n\left(\frac{Q}{\sqrt{2}}\right)$$

in its own hemisphere, and

$$N_{opp} = n(Q) - n\left(\frac{Q}{\sqrt{2}}\right) \simeq \ln\sqrt{2} \cdot n'(Q) = \mathcal{O}\left(\sqrt{\alpha_s}\, n(Q)\right)$$

particles backwards. This does not affect the total multiplicity of an event, since the missing piece in the quark's hemisphere is covered by an identical contribution from antiquark backward radiation.

However, these two parts, while flying in the same direction, are independent by origin. They do not participate in a single cascade and therefore do not contribute to the P-KNO phenomenon.

3.8 Tails up!

The multiplicity distributions presented in [4] were plotted on a linear y-scale and looked uneventful. However, focusing on the tails of the log-plots of the same data in Fig.8 hints at a curious feature: very high-multiplicity fluctuations seem to occur more often than would be expected. Apparently something strange is going on on the high-multiplicity end when the multiplicity ratio hits $\nu = 3 \ldots$

The remaining four lowest-p_t ATLAS intervals $p_t \leq 500\,\mathrm{GeV}$ confirm the suspicion.
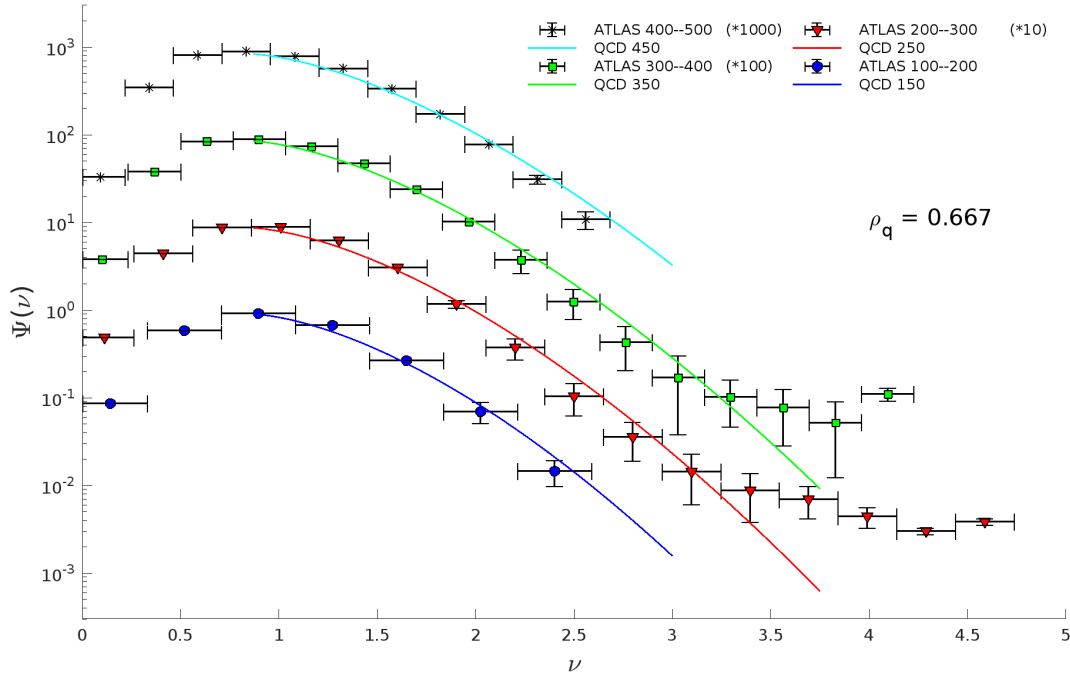
Figure 11: Charged hadrons in ATLAS jets: $100\,\mathrm{GeV} \leq p_{t,\mathrm{jet}} \leq 400\,\mathrm{GeV}$

ATLAS multiplicity distributions were discussed in a recent review [28] devoted to the KNO phenomenon. However, the authors skipped the intervals $p_t = 200$–300 and 300–400 GeV, the ones where this misbehaviour is most prominent. The two middle sets in Fig. 11, in our opinion, leave no doubt that the "*tails up*" feature that can be seen in almost every data set is not an unfortunate glitch in the estimate of systematics, but rather some new unexpected phenomenon worth exploring.

We therefore turn to a discussion of the possible origin — and the possible impact — of *flattening* of the rate of high multiplicity fluctuations.

4   ATLAS tail and CMS ellipticity

4.1 ATLAS high-p_t jets

4.1.1 Large-multiplicity bias: angular push
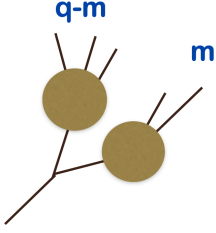
Figure 12: Topology of large-ν measurement

Selecting events with an abnormally large multiplicity creates a bias. In order to see that, let us look into the angular and energy pattern of parton splittings that form such events.

The characteristic rank of multiplicity moment that governs the yield of events at a given ν was estimated above as

$$k_{\rm sd} \sim \mu\big[D(\gamma)\nu\big]^{\mu} \tag{4.1}$$

where $\mu = 1/(1-\gamma) \sim 1.7$. With ν increasing we start to probe higher and higher multiplicity moments $q \sim k_{\rm sd}$.

Now consider the Evolution Equation for the multiplicity moments. It has the following structure [2]

$$g_q \sim \int^{\Theta} \frac{d\theta'}{\theta'} \sum_{m=1}^{q-1} C_q^m g_m g_{q-m} \int_{\delta'}^{1-\delta'} \frac{dz}{z} \gamma^2(k_\perp) \frac{N^m(zE\theta')N^{q-m}((1-z)E\theta')}{N^q(E\Theta)}, \quad \left(\delta' = \frac{Q_0}{E\theta'}\right) \tag{4.2}$$

where scaling was envisaged, $n_m(Q) = g_m \cdot [N(Q)]^m$.

The multiplicity factors N in (4.2) are growing functions of the argument proportional to θ'. As a result, integration over the angle θ' of the splitting converges, and the collinear cutoff parameter δ' can be dropped. Since in the essential integration region $\ln(\Theta/\theta')$ is finite, we can approximate the multiplicity factors as

$$\ln N(\theta'E) \;=\; \ln N(E) + \ln\frac{\theta'}{\Theta} \cdot \frac{dN(E\Theta)}{d\ln E} + \mathcal{O}\big(\gamma^2\big), \tag{4.3}$$

$$N(\theta'E) \;\simeq\; \left(\frac{\theta'}{\Theta}\right)^{\gamma} \cdot N(E). \tag{4.4}$$

Substituting into (4.2) results in

$$\sim \int^{\Theta} \frac{d\theta'}{\theta'} \left(\frac{\Theta}{\theta'}\right)^{-q\gamma} \times \sum_{m=1}^{q-1} C_q^m g_m g_{q-m} \int_{\delta}^{1-\delta} \frac{dz}{z} \gamma^2 \frac{N^m(zE\Theta)N^{q-m}((1-z)E\Theta)}{N^q(E\Theta)}, \tag{4.5}$$

The entire dependence on θ' is now localised in a simple integral:

$$I(\gamma q) = \int^{\Theta} \frac{d\theta'}{\theta'} \left(\frac{\Theta}{\theta'}\right)^{-q\gamma} = \frac{1}{\gamma q}. \tag{4.6}$$

We may characterise the typical "angular distance" between the splitting and the jet opening angle by an average pseudorapidity distance[1]

$$\Delta\eta^* \sim \left\langle \ln\frac{\Theta}{\theta_1} \right\rangle = I^{-1}\int^{\Theta} \frac{d\theta'}{\theta'} \ln\frac{\Theta}{\theta'} \left(\frac{\Theta}{\theta'}\right)^{-q\gamma} = -\frac{1}{I}\frac{d\,I(\alpha)}{d\alpha}\bigg|_{\alpha=\gamma q} = \frac{1}{q\,\gamma}. \tag{4.7}$$

It is supposed to be large, since formally $\gamma \propto \sqrt{\alpha_s}$ is a small PT-expansion parameter. As we know, the anomalous dimension floats between 0.3 (corresponding to the maximal foreseeable hardness, of the order of 10 TeV) up to $\gamma \lesssim 0.6$ (for $Q \sim 10\,{\rm GeV}$), see Fig. 3. In real life $\gamma \in \frac{1}{3} \div \frac{1}{2}$. When studying jet multiplicity, $q=1$, the pseudo-rapidity difference is still significant, $\Delta\eta^* > 2$ (for smaller hardness scales Q) or even $\Delta\eta^* > 3$ (the largest Q) .

However, when one turns to multiplicity moments, the situation changes drastically: already for multiplicity ranks $q \geq 2 \div 3$ one has $\Delta\eta^* < 1$. This means that the first parton splitting gets pushed out more the larger the moment rank one considers.

---

[1]η^* stands for pseudorapidity with respect to the parent parton, measured along the jet axis.

4.1.2 Large-multiplicity bias: energy share

A similar bias occurs in the pattern of parton energy sharing.
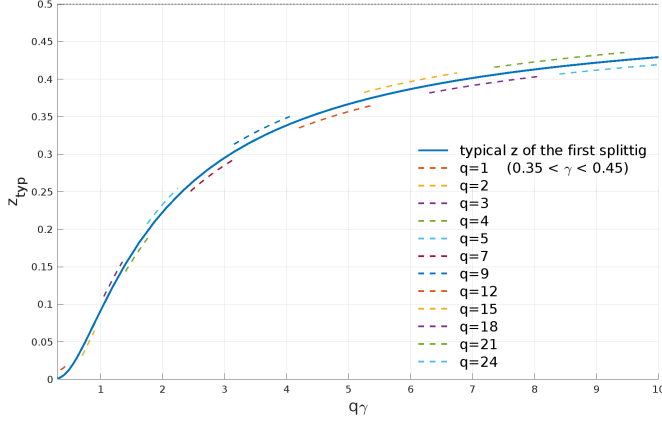

Figure 13: Typical energy share as a function of $q\gamma$

From the structure of the z integral in (4.5),

$$\sum_m^q C_q^m g_m g_{q-m} \times \int \frac{dz}{z} \, z^{m\gamma} (1-z)^{(q-m)\gamma},$$

and recalling the multiplicity moments (2.9), it is straightforward to deduce (using similar trick of partial differentiation over $m\gamma$ while keeping $(q-m)\gamma$ fixed)

$$\left\langle \ln \frac{1}{z} \right\rangle \simeq \psi(1+q\gamma) - \psi(\langle m \rangle \gamma) \quad (4.8a)$$

with

$$\langle m \rangle \simeq \frac{\sum_m^q m^2(q-m)}{\sum_m^q m(q-m)} = \frac{1}{2}q. \quad (4.8b)$$

Soft gluons are forced to carry an energy fraction larger than they were used to in average unbiased jets. As the rank q increases, the logarithmic z-integration gets squeezed. In two obvious limits (4.8) tells us

$$\left\langle \ln \frac{1}{z} \right\rangle \quad \simeq \quad \frac{2}{q\gamma}, \qquad q\gamma \ll 1, \quad (4.9a)$$

$$\rightarrow \quad \ln 2, \qquad q\gamma \gg 1. \quad (4.9b)$$

According to (4.9b) in the asymptotic limit $q \to \infty$ energy equilibration is reached, $z \to \frac{1}{2}$, while for finite ranks and small coupling the gluon stays soft and free to provide a logarithmic enhancement.

This effect is displayed in Fig. 13 where the typical bremsstrahlung gluon energy fraction z_{typ} is shown by the solid curve.

Dashed lines mark the domains of z_{typ} corresponding to the values of q from 1 to 6 in the most interesting range $\gamma \, 0.35 \div 0.45$. The soft gluon turns hard and the logarithmic enhancement goes away. For example, $z_{\text{typ}} = \frac{1}{3}$ around $q\gamma \approx 4$.

The last step to take is to estimate the rank of the multiplicity moments q that determine the P-KNO distribution at a given ν. The characteristic moment $q_{\text{char}}(\nu)$ can be estimated from the position of the steepest-descent point in the defining integral

$$g_q = \int_0^\infty d\nu \, \nu^q \, \Psi^{(\rho)}(\nu, \gamma). \quad (4.10)$$

Substituting (2.18) and looking for a maximum in $\ln \nu$, gives an estimate

$$q_{\text{char}}(\nu) \simeq \mu \left(\rho \cdot [D\nu]^\mu - \frac{3\rho - 1}{2} \right) = \rho k_{\text{sd}} + \frac{1}{2}\mu. \quad (4.11)$$

14

The resulting relationship between ν and q_{char} depends on the nature of the jet (ρ) and changes with the hardness scale via the dependence of D and μ on γ.

Fig. 14 displays this relation for a quark jet ($\rho = \rho_q = \frac{2}{3}$).

Assuming the jet radius $R \simeq 0.8$, the hardness scale of the two spectacularly misbehaving p_t intervals translates to $Q \sim 200 \div 270\,\text{GeV}$. The anomalous dimension at this scale is $\gamma(\alpha_s(Q)) \approx 0.39$. The corresponding curve is marked by circles.

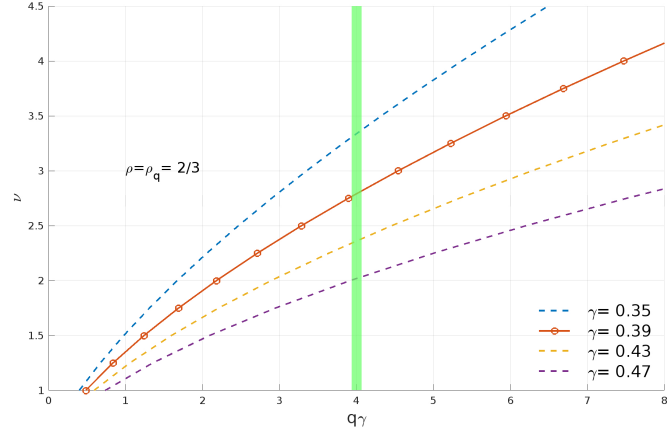The squeeze value $q_{\text{char}}\gamma \simeq 4$ (the green line) is reached when $\nu \simeq 2.75$.

Figure 14: ν as a function of $q_{\text{char}}\gamma$

4.1.3 Tail flattening

At this point, nothing bad happens to the QCD expression (2.18) for the tail. It still describes multiplicity fluctuations *in a quark jet* dressed up with secondary collinear/soft partons.

What really changes above $\nu = 2.5$ is the *nature of the object under study*: it is a single jet no longer.

As can be seen in Fig. 11 the tail shape changes above $\nu \simeq 3$. Apparently, the interval between $\nu = 2.5$ and $\nu = 3$ is the transition region.

For still larger ν one should look upon the jet as a two-jet system $(q + g)$ as a source of new particles. Its "source strength" is larger than that of the original quark, $\rho \to \rho + 1$, and the tail flattens.

This conclusion might look surprising, since according to (2.18) the fluctuation distribution should get *narrower* with an increase of ρ. True, *provided* for each jet or system of jets we calculate ν by normalizing the number of particles by the proper mean,

$$\nu = \frac{n}{\left\langle n^{(\rho)} \right\rangle}. \tag{4.12a}$$

What we are doing instead is counting particles in units of the original quark jet multiplicity in place of a larger split-tongue multiplicity,

$$\nu = \frac{n}{\left\langle n^{(\rho_q)} \right\rangle}. \tag{4.12b}$$

As a result the characteristic exponent gets *smaller* when ρ_q is replaced by a larger $\rho = \rho_q + 1$:

$$-\rho \cdot \left(\nu\right)^{\mu} = -\rho \cdot \left(\frac{n}{\left\langle n^{(\rho)} \right\rangle}\right)^{\mu} = -\rho^{1-\mu} \cdot \left(\frac{n}{\left\langle n_g \right\rangle}\right)^{\mu} \propto -\rho^{-\gamma\mu} \simeq -\rho^{-\frac{2}{3}} \quad (\text{for } \gamma = 0.4). \tag{4.13}$$

The change in slope does not occur abruptly. At the moment, it is not clear to us how to treat the tail-up transition quantitatively.

Meanwhile, it seems plausible that the resolution of the ATLAS puzzle may be related to the "rattlesnake effect" (RSE) at which we are pointing (split tongue causing a raised tail).
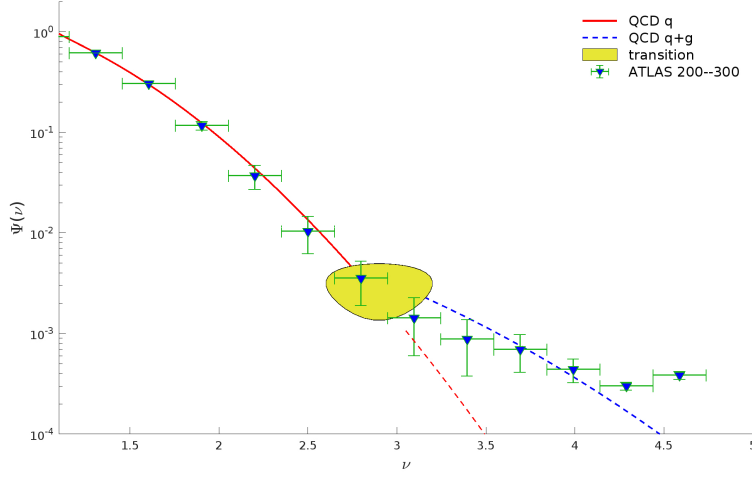
Figure 15: Tail-up transition around $\nu = 3$

To support this hypothesis, Fig. 15 shows what is about to happen when a quark jet is replaced by a pair $q+g$ with comparable hardness.

The standard one-quark curve (red) is $\Psi^{(\rho_q)}(\nu)$, and the quark+gluon one (dashed blue) corresponds to

$$\Psi^{(\rho_q+1)}(x) \times \Psi^{(\rho_q)}(3)$$

evaluated at

$$x = \frac{\nu}{\rho_q+1}.$$

4.2 Snake-tongue transition and CMS high-multiplicity jets

'Why, sometimes I've believed as many as six impossible things before breakfast' [1]

There is another puzzle for which RSE may assume responsibility.
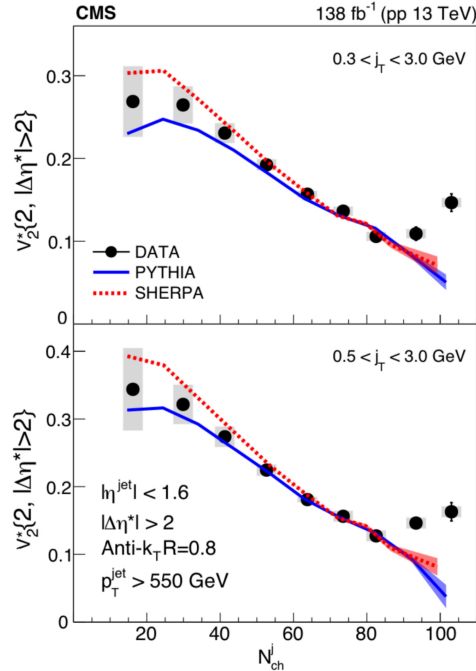
Figure 16: v_2^* versus jet multiplicity [3]

The CMS Collaboration recently found a spectacular change in the trend of the behaviour of the second azimuthal harmonic v_2^* of long-range ($|\Delta\eta^*| > 2$) two-particle correlations [3].

On our side we make the following observation:

Divided by the mean multiplicity $N_{\mathrm{ch}}^j \simeq 26$ reported by CMS, the turning point in Fig. 16 translates into

$$\nu = 80/26 \simeq 3.$$

Given that the hardness scales of CMS $p_t > 550$ GeV jets and the snaky ATLAS jets discussed above are close, it is worth looking into the possibility that the two – equally crazy – phenomena have a common origin: the RSE scenario.

As far as a split tongue goes together with a raised tail, it seems natural to refer to this picture as RSE.
The name is flexible, as it can be read as "rattlesnake event", or "rattlesnake effect", depending on context.

4.2.1 Jet finder at work

Imagine we had two hard partons with comparable energies (1:2) flying apart at a 45° angle.

What will the final state look like?

16

The anti-kt machinery first collects secondary particles in the 30+30 degree cone around the hardest primary parton (quark), labeled "anti-kt borderline" in Fig. 17.

Then it assembles the second bunch around the less energetic parton from inside the 15+15 degree cone.

Having done so, the algorithm will combine the two freshly cooked subjets into one, as long as their angular distance is less than the chosen "radius" $R = 0.8$.
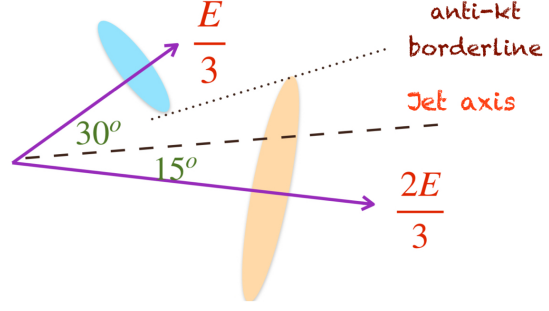
Figure 17: Snake-tongue jet substructure

The jet axis is determined with respect to which the rapidity η^* and the azimuthal angle ϕ^* are measured. *Note:* here and in what follows, variables marked with a star are defined with respect to the jet axis, and j_t refers to the transverse momentum of a hadron with respect to it [31,3]

4.2.2 Jet axis misused

"When I use a word, it means just what I choose it to mean — neither more nor less" [1]

The "jet axis" is purely formal: It points in the direction of an aggregate jet momentum, but it has little to do with the physics of radiation.

Let us take the two-parton configuration of Fig. 17 as a toy model to see what kind of effects one should expect in the snake-tongue event scenario.

Expectation 1: In usual unbiased events the jet axis practically coincides with the direction of the quark momentum. In this situation, one should see a "Feynman plateau" in the inclusive distribution in η^*.

Expectation 2: As a consequence of pQCD cascades, the height of this plateau should slowly but steadily increase towards smaller η^* as

$$\frac{dn}{d\eta^*} \simeq \frac{d}{d\eta^*} N_q \left(E_{\text{jet}} \sin \frac{\theta}{2} \right) = \frac{d}{d\eta^*} N_q \left(fracE_{\text{jet}} \sqrt{1 + \exp(2\eta^*)} \right). \tag{4.14}$$

Expectation 3: In RSE instead, the bulk of offspring are radiated off the two hard partner partons that are away from the axis. Since radiation is predominantly collinear to their respective parents, the produced particles will peak at two η^* values that correspond, in the particular kinematics of Fig. 17, to 15 and 30 degree angles to the "jet axis", $\eta^* = 2.1$ and $\eta^* = 1.3$.

So, a significant enhancement should be expected at $\eta^* \sim 1 \div 2$ because it is the region covered by the snake tongue, where most secondary radiation flies.

Expectation 4: For the same reason, the η^*-distribution should drop to $\exp(-2\eta^*)$ because the radiated particles can align with the axis only by accident (phase space).

Expectation 5: Turning from inclusive distribution to particle correlations, the RSE is a planar event with its jet axis lying in the plane between the quark and the gluon. Therefore, among hadron pairs half will belong to subjets that are on opposite sides with respect to the jet axis. Massive $\phi^* = \pi$ correlations are expected.

Expectation 6: Since RSEs coexist with normal events with one quark as the leader, the opposite-side correlations must grow when one cuts out "small transverse momenta" hadrons, $j_t > [j_t]_{min} =$ few hundred MeV. This would increase the portion of RSE in the event sample. Since "baby snakes" are omnipresent as rare fluctuations, imposing a j_t-cut will increase back-to-back correlations for any multiplicity, not necessarily extremely large.

Expectation 7: Starting from the point where RSE becomes dominant, a j_t-cut should no longer matter.

All these expectations are met by the CMS data.

Expectations # 1 to 4 find confirmation in the inclusive pseudorapidity distribution of charged hadrons [3,29] shown in Fig. 17.

A plateau is manifest in normal jets with multiplicity of hadrons close to the mean (red points).

Its increase towards smaller η^* values is seen.

In contrast, in the high-multiplicity event sample (blue points), the RSE is in action, and the jet axis no longer represents the direction of any hard parton, causing the η^* distribution to fall exponentially, demonstrating that a small angle of a hadron with respect to the jet axis is an accident rather than the norm.

The particle density is by an order of magnitude higher at $\eta^* = 1 \div 2$ than in unbiased events, the ones that are not forced to produce an exceptionally large multiplicity.
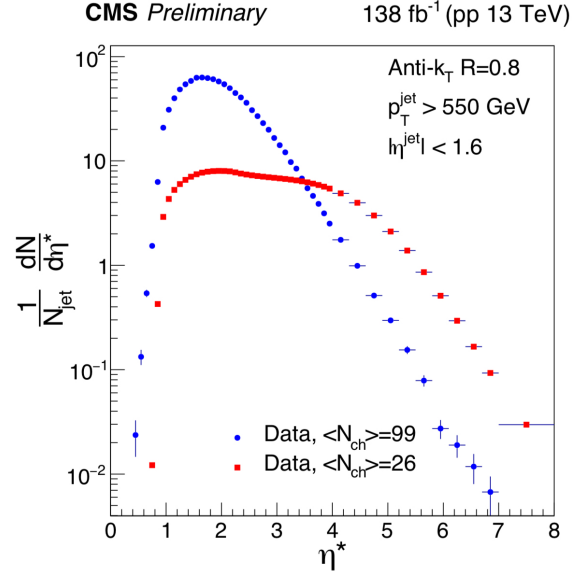
Figure 18: Large-η^* tail $\propto \exp(-2\eta^*)$.

Now we move to correlations.

Expectation # 5 is what Fig. 16 is all about: increase of opposite-side azimuthal correlations with increase of registered multiplicity as a means of enriching the proportion of RSE.
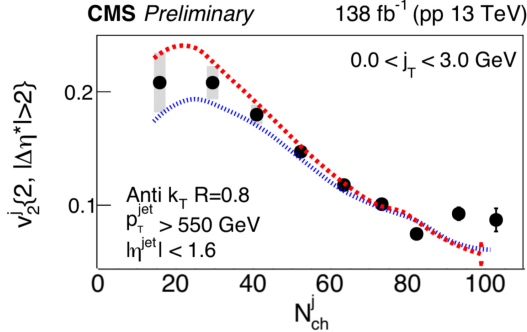
Figure 19: No-j_t-cut data [29]

Expectations # 6 and 7 find support in the comparison of the two panels of Fig. 16, published in the CMS article [3], with a third that was presented in [29]: Fig. 19 taken from the latter shows the measurement of v_2^* without imposing a j_t cut.

Compared with Fig. 16, the turnover at $N \sim 80$ is less pronounced and, more importantly, v_2^* is systematically larger in Fig. 16 than in Fig. 19 for *all* multiplicities.

This shows that "baby snakes" are an intrinsic part of parton cascades.

Below $N_{ch}^j \sim 80$ ($\nu \simeq 3$), the cut-off value is important: Moving from $[j_t]_{min} = 0$ to 0.3 and then to 0.5 GeV causes a steady increase in v_2^*.

Starting from $\nu \sim 3$, the value of $[j_t]_{min}$, 0.3 or 0.5, no longer makes any difference because a cut leaves snake-tongued configurations unaffected.[2]

By then, baby snakes have matured and started to take over.

4.2.3 Long-range away ridge

The last point to pay attention to is whether the opposite-side correlations that the RSE generates are good enough to qualify as "long-range" ($|\Delta\eta^*| > 2$).

---

[2] *Remark:* Apparently, the upper bound on the transverse momenta of hadrons was inherited from an earlier study of collective effects where $p_t < 3\,\text{GeV}$ was chosen to minimize correlations from jets while studying minimum bias events [30]. In the present context, it is irrelevant.

Figure 20: Large-η^* particles as a misunderstanding

Recall that the RSE triggers a *plane* in the jet fragmentation phase space and produces two peaks in η^* that are always opposite in azimuth. Depending on whether the two triggered hadrons are picked from the same subjet or from opposite subjets, one obtains same-side or opposite-side correlations.

If subjets were pencil-like, we would have short-range forward correlations in rapidity, $|\Delta\eta^*| \simeq 0$ ($\phi^* = 0$). The opposite side, in contrast, has a handicap: the varying opening angle of the emitters guarantees an initial ridge with a width of the order 1, $|\Delta\eta^*| = 1.3 - 2.1 = 0.8$. This spread can be made larger by allowing the gluon to carry a somewhat smaller momentum fraction.
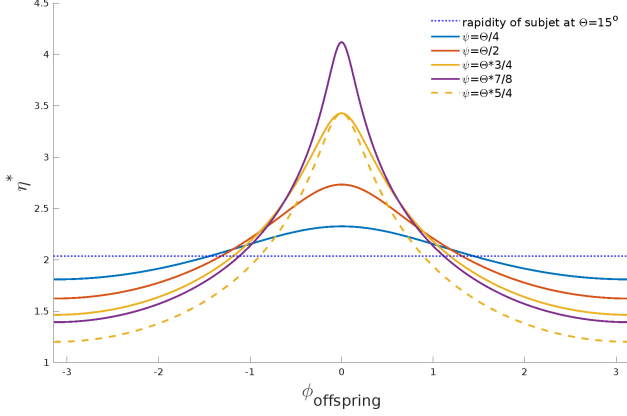
Another source of extending the rapidity span of the ridge is QCD bremsstrahlung. It is spread in angles, so that some part of the accompanying radiation may accidentally hit the "axis" direction and will be interpreted as having a large η^*.

Fig. 20 demonstrates this effect. Here, Θ is the angle of the leading quark to the jet axis and ψ, $\phi_{\text{offspring}}$ are the polar and azimuthal angles of the secondary radiation with respect to its quark parent. The solid curves ($\psi < \Theta$) show the rapidity spread in back-to-back correlations (the dashed line ($\psi > \Theta$) gives an example of an additional contribution to the same-side correlation spread).

The pseudorapidity of the harder parton (the quark with $2/3E$ in Fig. 20) is marked by the dotted line. Picking up an offspring of the quark subjet and correlating it with any of an offspring of the second subjet (with smaller η^*) will generate a $\phi^* \sim \pi$ effect. Given the relative proximity of the quark to the jet axis, such an induced long-range correlation can be quite significant and spread in $|\Delta\eta^*|$.

A simple phase-space probability estimate leads to an exponential drop-off at large relative rapidity $dw \propto \exp(-2|\Delta\eta^*|)$.

Should the RSE picture prove viable, one may expect the fork structure of the leading partons to progress further with increasing ν, from trident to "used shaving brush". The away ridge will first become shorter in η^* and then recede, causing v_2^* to decrease again, leaving room for higher harmonics.

5 Conclusions

> Alice: Would you tell me, please, which way I ought to go from here?
> The Cheshire Cat: That depends a good deal on where you want to get to.
> Alice: I don't much care where...
> The Cheshire Cat: Then it doesn't much matter which way you go.
> Alice: ...So long as I get somewhere.
> The Cheshire Cat: Oh, you're sure to do that, if only you walk long enough [1]

We have presented arguments in favour of the QCD picture of particle multiplication in hard interactions, by confronting with experiment the analytic perturbative QCD formulas describing multiplicity fluctuations (the Polyakov–Koba–Nielsen–Olesen scaling phenomenon).

An unconventional ingredient has been introduced into our approach:

> Using an expression for the P-KNO distribution, we replaced the ratio of quark and gluon *colour charges* / by the experimental ratio of quark and gluon jet *hadron multiplicities*.

This move allowed us to describe high-end multiplicity fluctuations both in e^+e^- (full event and one-hemisphere distributions) and in LHC high-p_t jets. The analytic prediction of the height and shape of the P-KNO tail agrees reasonably well with the data from e^+e^- annihilation and LHC high-p_t jets, despite having no tunable parameters.

Analysing the tails of multiplicity distributions measured by the ATLAS Collaboration, we dwelt on a certain flattening of the falloff above $\nu \simeq 3$, and proposed a possible qualitative explanation for this phenomenon.

We also linked it with another puzzling observation recently reported by the CMS Collaboration: the growth of long-range back-to-back correlations with increase of hadron multiplicity inside high-p_t jets.

The CMS discovery was triggered by a theoretical suggestion to look for signs of collective effects inside jets as a result of final-state interaction between partons. Quote [3]:

> "The non-monotonic dependence of v_2^* versus N_{ch}^j [$\cdots$] may indicate an onset of novel QCD phenomena related to nonperturbative dynamics of a parton fragmenting in the vacuum. These phenomena could include the emergence of collective effects possibly driven by final-state rescatterings, as suggested in Ref. [31]"

However, hunting for collective "QGP-like" phenomena inside a QCD jet propagating in the vacuum is doomed to fail. This follows from an old analysis of the space-time picture of perturbative multiplication of QCD partons. This conclusion motivated the hypothesis of local parton–hadron duality (LPHD [14,32]), which has been experimentally verified since then and continues to march with flying colours today.

In simple terms, reinteraction between partons inside the jet would contradict causality. Two partons originating from a QCD cascade, either having a common parent or coming from separate branches, created simultaneously or at different time scales, have a space-like interval between them and cannot talk to (let alone collide with) one another.

Our alternative explanation, the "rattlesnake effect", RSE, is straightforward to reject/validate experimentally. All one needs to do is look into the *internal structure* of jets selected for an abnormally large hadron multiplicity.[3]

To conclude, similar phenomena, namely, the slowing of the falloff of the P-KNO distribution and the funny behaviour of v_2^* should manifest themselves in e^+e^- annihilation as well, when/if the data on rare multiplicity fluctuations with $n/\langle n \rangle > 3$ become available. As we show in Fig. 21, presently available e^+e^- data run out of statistics just where the enhanced tail should start to become apparent. One may hope for confirmation/refutation of the RSE hypothesis from resurrected LEP or future e^+e^- collider data.

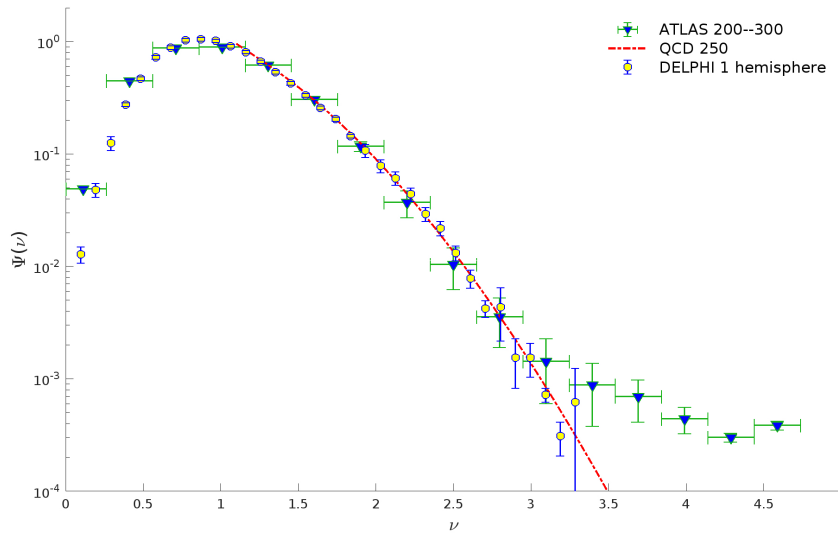Figure 21: ATLAS and DELPHI jets with comparable hardness

---

[3]After this paper was completed, we learned of a forthcoming CMS publication [33] in which the possibility of two-pronged structure of ellipticity generating events is put under scrutiny.

References

1. Lewis Carroll, "Alice's Adventures in Wonderland", 1865.

2. Yu.L. Dokshitzer, "Improved QCD treatment of the KNO phenomenon",
   Phys.Lett. <u>305 B</u> (1993) 295.

3. CMS Collaboration, "Observation of enhanced long-range elliptic anisotropies inside high-multiplicity jets in pp collisions at $\sqrt{s}$ 13 TeV", *Phys.Rev.Lett.* <u>133</u> (2024) 142301.

4. G. Aad et al. [ATLAS], *Phys.Rev.* <u>D100</u> (2019) 052011.

5. A.M. Polyakov, "A Similarity hypothesis in the strong interactions. 1. Multiple hadron production in e+ e- annihilation", *Sov.Phys.JETP* <u>32</u> (1971) 296;
   "Similarity hypothesis in strong interactions. 2. Cascade formation of hadrons and their energy distribution in e+ e- annihilation", *ibid.* <u>33</u> (1971) 850.

6. Z. Koba, H.B. Nielsen and P. Olesen, "Scaling of multiplicity distributions in high-energy hadron collisions", *Nucl.Phys.* <u>B40</u> (1972) 317.

7. A. Bassetto, M. Ciafaloni and G. Marchesini, "Jet Structure and Infrared Sensitive Quantities in Perturbative QCD", *Phys.Rep.* <u>100</u> (1983) 201.

8. Yu.L. Dokshitzer, V.S. Fadin and V.A. Khoze, "Double Logs of Perturbative QCD for Parton Jets and Soft Hadron Spectra", *Zeit.Phys.* <u>C15</u> (325) 1982.

   https://www.lpthe.jussieu.fr/~yuri/BPQCD/BPQCD.pdf

9. Yu.L. Dokshitzer, V.A. Khoze, A.H. Mueller and S.I. Troyan, *Basics of Perturbative QCD*, ed. J. Tran Thanh Van, (Editions Frontières, 1991).

   https://www.lpthe.jussieu.fr/ yuri/BPQCD/BPQCD.pdf

10. E.D. Malaza and B.R. Webber, "QCD Corrections to Jet Multiplicity Moments", *Phys.Lett.* <u>149B</u> (1984) 501.

11. E.D. Malaza and B.R. Webber, "Multiplicity Distributions in Quark and Gluon Jets", *Nucl.Phys.* <u>B267</u> (1986) 702.

12. F. Cuypers and K. Tesima, "Resummed multiplicity moments", *Zeit.Phys.* <u>C54</u> (1992) 87.

13. A.H. Mueller, "Multiplicity and Hadron Distributions in QCD Jets: Nonleading Terms", *Nucl.Phys.* <u>B213</u> (1983) 85

14. Yu.L. Dokshitzer and S.I. Troyan, "Asymptotic Freedom and Local Parton–Hadron Duality", Proceedings of the XIX Winter School of the LNPI, vol. 1, page 144. Leningrad, 1984.

15. E.D. Malaza, "Multiplicity distributions in quark and gluon jets to $\mathcal{O}(\alpha_s)$",
    Zeit.Phys. <u>CC31</u> (1986) 143.

16. B.R. Webber, "Average Multiplicities in Jets", *Phys.Lett.* <u>143B</u> (1984) 501

17. S. Catani, G. Marchesini and B.R. Webber, "QCD coherent branching and semiinclusive processes at large x", *Nucl.Phys.* <u>B349</u> (1991) 635.

18. Yu.L. Dokshitzer, V.A. Khoze and S.I. Troian, "Specific features of heavy quark production. LPHD approach to heavy particle spectra", *Phys.Rev.* <u>D53</u> (1996) 89.

19. J. Abdallah et al. [DELPHI], "Charged particle multiplicity in three-jet events and two-gluon systems", *Eur. Phys.J.* <u>C44</u> (2005) 311.

20. G. Abbiendi et al. [OPAL], "Particle multiplicity of unbiased gluon jets from e^+e^- three jet events", *Eur. Phys.J.* <u>23</u> (2002) 597.

21. M.S. Alam, et al. [CLEO], "Study of gluon versus quark fragmentation in $\Upsilon \to gg\gamma$ and $e^+e^- \to q\bar{q}\gamma$ events at $\sqrt{s} = 10$ GeV", *Phys.Rev.* <u>D56</u> (1997) 17.

22. D. Buskulic, et al. [ALEPH], "Quark and gluon jet properties in symmetric three-jet events", *Phys.Lett.* <u>384B</u> (1996) 353.

23. P.D. Acton, et al., The OPAL collaboration, "A Study of charged particle multiplicities in hadronic decays of the Z0", *Zeit.Phys.* <u>CC 53</u> (1992) 539 .

24. P. Abreu, et al. The DELPHI collaboration, "Production of charged particles, K0(s), K+-, p and Lambda in Z –> b anti-b events and in the decay of b hadrons", *Phys.Lett.* <u>B 347B</u> (1995) 447.

25. W. Braunschweg, et al., The TASSO collaboration, "Charged Multiplicity Distributions and Correlations in e^+e^- Annihilation at PETRA Energies", *Zeit.Phys.* <u>CC 45</u> (1989) 193.

26. Yu.L. Dokshitzer, S.I. Troian and V.A. Khoze, "Multiple hadroproduction in hard processes with nontrivial topology. (In Russian)", *Sov.J.Nucl.Phys.* <u>47</u> (1988) 881 ;
P. Eden, G. Gustafson and V.A. Khoze, "On particle multiplicity distribution in three jet events", *Eur. Phys.J.* <u>11</u> (1999) 345.

27. M. Cacciari, G.P. Salam and G. Soyez, "The anti-k_t jet clustering algorithm",
Journal of High Energy Physics, Volume 2008, JHEP04(2008).

28. G.R. Germano, F.S. Navarra, G. Wilk and Z. Wlodarczyk, "Emergence of Koba-Nielsen-Olsen scaling in multiplicity distributions in jets produced at the LHC", *Phys.Rev.* <u>D110</u> (2024) 034026 .

29. Parker Gardner on behalf of the CMS collaboration, "Observation of QCD collectivity inside high-multiplicity jets in pp collisions with the CMS experiment", Talk at Quark Matter, Sept. 2023.

https://cds.cern.ch/record/2862457/files/HIN-21-013-pas.pdf

30. V. Khachatryan et al. [CMS], "Evidence for collectivity in pp collisions at the LHC",
Phys.Lett. <u>B765B</u> (2017) 193.

31. A. Baty, P. Gardner and W. Li, "Novel observables for exploring QCD collective evolution and quantum entanglement within individual jets", *Phys.Rev.* <u>CC107</u> (2023) 064908.

32. Ya.I. Azimov et al., "Similarity of Parton and Hadron Spectra in QCD Jets",
Zeit.Phys. <u>C27</u> (1985) 65.

33. The CMS Collaboration, "Unveiling the dynamics of long-range correlations in high-multiplicity jets through substructure engineering in pp collisions at CMS", CMS PAS HIN-24-024.

34. Yu.L. Dokshitzer,"Bremsstrahlung", Contribution to: 11th NATO Advanced Study Inst. on Techniques and Concepts of High-Energy Physics, H.B. Prosper, B. Harrison and M. Danilov (ed), NATO Sci. Ser. <u>C 566</u> (2001) 51.

35. Gergö Nemes, "New asymptotic expansion for the Gamma function", Archiv der Mathematik, Volume 95 (2010) 161.

Appendices

A   Accuracy of the asymptotic P-KNO model

Factorial moments are generated by Taylor expansion of the Laplace transform about the origin:

$$\Phi(-\beta) = \sum_{k=0}^{\infty} \frac{\beta^k}{k!} \, g_k. \tag{A.1}$$

The DLA moments of the gluon jet multiplicity distribution come from the corresponding recurrence relation [8,9]

$$\Phi(-\beta) = 1 + \beta + \frac{4}{3}\frac{\beta^2}{2!} + \frac{9}{4}\frac{\beta^3}{3!} + \frac{208}{45}\frac{\beta^4}{4!} + \frac{2425}{216}\frac{\beta^5}{5!} + \dots \tag{A.2}$$

Moments of high rank $k \gg 1$ are determined by the singularity of Φ positioned at $z = -\beta/C = 1$:

$$\Phi^{\mathrm{as}}(-\beta) = 2\left[\frac{z}{(1-z)^2} - \frac{1}{3}\ln(1-z)\right] + \mathcal{O}(1). \tag{A.3}$$

Expanding this formula near $z = 0$ produces the asymptotic moments (2.3). Eq. (A.3) was derived for z close to 1 to describe high-rank moments. Nevertheless, one can attempt to apply it to all moments, including low-rank ones. To do that, it suffices to adjust (A.3) to ensure the correct normalization, $g_0 = 1$, by fixing the $\mathcal{O}(1)$ term:

$$\Phi^{\mathrm{as}}(-\beta) = 1 + 2\left[\frac{z}{(1-z)^2} - \frac{1}{3}\ln(1-z)\right] = 1 + 2\sum_{k=1}^{\infty}\left[k + \frac{1}{3k}\right]\left(\frac{\beta}{C}\right)^k, \tag{A.4}$$

$$g_k^{\mathrm{DLA}} = \frac{2k!}{C^k}\left(k + \frac{1}{3k}\right). \tag{A.5}$$

For a quark jet or jet ensemble with effective "colour charge" ρ, the Laplace transform becomes

$$\Phi^{(\rho)}(-\beta) = \sum_{k=0}^{\infty}\frac{\beta^k}{k!}g_k^{(\rho)} = \left[\Phi\left(\frac{-\beta}{\rho}\right)\right]^{\rho}. \tag{A.6}$$

Substituting the expansions (A.2) and (A.4) one can compare the first few factorial moments coming from the exact solution and the large-k asymptotic formula for any jet ensemble.

A.1 Gluon jet

	recurrence	numeric	asymptotic	numeric
g_1	1	1.000	$\frac{8}{3C}$	1.045
g_2	$\frac{4}{3}$	1.333	$\frac{26}{3C^2}$	1.330
g_3	$\frac{9}{4}$	2.250	$\frac{112}{3C^3}$	2.244
g_4	$\frac{208}{45}$	4.622	$\frac{196}{C^4}$	4.616
g_5	$\frac{2425}{216}$	11.227	$\frac{1216}{C^5}$	11.218

At large k the remainder is proportional to g_k/k^3.

A.2 Quark jet

For quark jet phenomenology, instead of the canonical 4/9 we use $\rho = 2/3$. This gives the following table

	recurrence	numeric	asymptotic	numeric
g_1	1	1.000	$\frac{8}{3C}$	1.045
g_2	$\frac{3}{2}$	1.500	$\frac{85}{9C^2}$	1.449
g_3	$\frac{49}{16}$	3.063	$\frac{1376}{27C^3}$	3.064
g_4	$\frac{319}{40}$	7.975	$\frac{27352}{81C^4}$	7.953
g_5	$\frac{3243}{128}$	25.336	$\frac{668498}{243C^5}$	25.380

A.3 e^+e^-

For e^+e^- phenomenology, we use $\rho = 4/3$. This gives the following table

	recurrence	numeric	asymptotic	numeric
g_1	1	1.000	$\frac{8}{3C}$	1.045
g_2	$\frac{5}{4}$	1.250	$\frac{149}{18C^2}$	1.270
g_3	$\frac{121}{64}$	1.891	$\frac{854}{27C^3}$	1.901
g_4	$\frac{1079}{320}$	3.372	$\frac{93059}{648C^4}$	3.382
g_5	$\frac{14227}{2048}$	6.947	$\frac{1466089}{1944C^5}$	6.958

In conclusion, we observe that the asymptotic approximation is already quite good even at $k = 1$, for all relevant values of ρ.

B Factor $\chi(k)$

B.1 Γ–miracles

Gergö Nemes proposed the following approximate formula [35]

$$\Gamma(z) \approx \sqrt{\frac{2\pi}{z}} \left(\frac{1}{e} \left(z + \frac{1}{12z - \frac{1}{10z}} \right) \right)^z. \tag{B.1}$$

A simpler (though less accurate at large z) approximation

$$\Gamma(z) = \sqrt{\frac{2\pi}{z}} \left(\frac{1}{e} \left(z + \frac{1}{12z} \right) \right)^z \cdot \left[1 + \mathcal{O}\left(\frac{10^{-3}}{z^3} \right) \right] \tag{B.2a}$$

does a fantastic job for small (but important!) values of the argument:

$$\Gamma(1) \quad \simeq \quad \frac{\sqrt{2\pi}}{e} \cdot \left(1 + \frac{1}{12} \right) \approx 0.998982 = 1 - \mathcal{O}\left(10^{-3}\right), \tag{B.2b}$$

$$\Gamma(2) \quad \simeq \quad \frac{\sqrt{\pi}}{e^2} \cdot \left(2 + \frac{1}{24} \right)^2 \approx 0.999898 = 1 - \mathcal{O}\left(10^{-4}\right). \tag{B.2c}$$

To improve the approximation of the interpolating factor $\chi(k)$ let us use

$$\Gamma(1 + z) \quad \approx \quad \sqrt{\frac{2\pi}{(1 + z)}} e^{-(1+z)} \left(z + 1 + \frac{1}{12(1 + z)} \right)^{1+z}$$

$$= \quad \sqrt{2\pi(1 + z)} e^{-(1+z)} (1 + z)^z \left(1 + \frac{1}{12(1 + z)^2} \right)^{1+z}. \tag{B.3}$$

B.2 Ratio of Γ functions

First we apply eq.(B.3) to $\Gamma(1 + \gamma k)$:

$$\Gamma(1 + \gamma k) \quad = \quad \frac{\sqrt{2\pi(1 + \gamma k)}}{e} e^{-\gamma k} (1 + \gamma k)^{\gamma k} \left(1 + \frac{1}{12(1 + \gamma k)^2} \right)^{1+\gamma k}$$

$$= \quad \frac{\sqrt{2\pi(1 + \gamma k)}}{e} \gamma^{\gamma k} \left(\frac{k}{e} \right)^{\gamma k} \left[1 + \frac{1}{\gamma k} \right]^{\gamma k} \cdot \left(1 + \frac{1}{12(1 + \gamma k)^2} \right)^{1+\gamma k} \tag{B.4a}$$

From here one easily gets

$$\Gamma(1+k) = \frac{\sqrt{2\pi(1+k)}}{e}\left(\frac{k}{e}\right)^{k}\left[1+\frac{1}{k}\right]^{k}\cdot\left(1+\frac{1}{12(1+k)^2}\right)^{1+k}, \tag{B.4b}$$

$$\Gamma(1+(1-\gamma)k) = \frac{\sqrt{2\pi(1+(1-\gamma)k)}}{e}(1-\gamma)^{(1-\gamma)k}\left(\frac{k}{e}\right)^{(1-\gamma)k}\left[1+\frac{1}{(1-\gamma)k}\right]^{(1-\gamma)k}$$

$$\cdot\left(1+\frac{1}{12(1+(1-\gamma)k)^2}\right)^{1+(1-\gamma)k}. \tag{B.4c}$$

Constructing the ratio of the Γ functions (B.4) one obtains

$$\frac{\Gamma(1+k)}{\Gamma(1+\gamma k)\Gamma(1+(1-\gamma)k)} = \frac{e}{\sqrt{2\pi}}\sqrt{\frac{1+k}{(1+\gamma k)(1+(1-\gamma)k)}}\cdot\left[\gamma^\gamma(1-\gamma)^{1-\gamma}\right]^{-k}$$

$$\cdot\left[1+\frac{1}{\gamma k}\right]^{-\gamma k}\times\frac{\left(1+\frac{1}{12(1+k)^2}\right)^{1+k}}{\left(1+\frac{1}{12(1+\gamma k)^2}\right)^{1+\gamma k}\left(1+\frac{1}{12(1+(1-\gamma)k)^2}\right)^{1+(1-\gamma)k}} \tag{B.5}$$

Here we have dropped two factors whose ratio is close to 1 for both small and large k:

$$\frac{\left[1+\frac{1}{k}\right]^{k}}{\left[1+\frac{1}{(1-\gamma)k}\right]^{(1-\gamma)k}} = \left.\frac{1}{1}\right|_{k=0} = \left.\frac{e}{e}\right|_{k\to\infty} = \left.1\right|_{\gamma\to0}.$$

We might simplify eq.(B.5) even further by disregarding the two factors in the "1/12" correction terms:

$$R_2 = \frac{\left(1+\frac{1}{12(1+k)^2}\right)^{1+k}}{\left(1+\frac{1}{12(1+(1-\gamma)k)^2}\right)^{1+(1-\gamma)k}}. \tag{B.6}$$

In this way, we would lose control of the relative correction $\mathcal{O}(k^{-1})$ in the tail while preserving the DLA limit ($\gamma\to0$) and the correct normalization (the $k=0$ moment). As a function of moment k, the ratio (B.6) departs from $R_2(0)=1$ by decreasing with a mild slope $R'(0)=-\gamma/12$, hits the minimal value $R_{\min}=1-\frac{\gamma}{12(1+\sqrt{1-\gamma})^2}$ at $k=\frac{1}{\sqrt{1-\gamma}}$ and then returns to unity as $1-\frac{\gamma}{(1-\gamma)k}$. The deviation of this ratio from unity might be as large as 8% in the unrealistic $1-\gamma\ll1$ region. In reality, this deviation does not exceed 1%. So the approximation $R_2=1$ seems reasonable.

The simplified χ factor becomes

$$\chi(k) = \sqrt{\frac{1+k}{(1+\gamma k)(1+(1-\gamma)k)}}\frac{e\left[1+\frac{1}{\gamma k}\right]^{-\gamma k}}{\sqrt{2\pi}}\cdot\left(1+\frac{1}{12(1+\gamma k)^2}\right)^{-(1+\gamma k)} \tag{B.7}$$

At the point responsible for proper normalization of the P-KNO function, the moment $k=0$, another miracle occurs in eq.(B.7) which also applies to $\gamma=0$ (the limiting P-KNO distribution or 'DLA'):

$$\chi(k=0) = \chi(\gamma=0) = \frac{e}{\sqrt{2\pi}}*\frac{12}{13} = 1.001019 \qquad \text{sic!} \tag{B.8}$$

B.3 Asymptotic limit $k\to\infty$

In the true asymptotic limit $k,\gamma k,(1-\gamma)k\gg1$

$$\chi(k) \to \frac{1}{\sqrt{2\pi\gamma(1-\gamma)k}}. \tag{B.9}$$

C Derivation of the P-KNO tail for a gluon jet

In this Appendix we show how to restore $\Psi(\nu)$ from its moments.

The moments (2.9) read

$$g_k = g_k^{\text{DLA}} \cdot \frac{[\Gamma(1+\gamma)]^k}{\Gamma(1+k\gamma)}, \qquad g_k^{\text{DLA}} = \frac{2k!}{C^k}\left(k+\frac{1}{3k}\right) \qquad (k \gg 1), \tag{C.1}$$

$$g_k = \frac{2}{\tilde{C}^k}\left(k+\frac{1}{3k}\right) \cdot \frac{k!}{\Gamma(1+\gamma k)}, \qquad \text{with} \quad \tilde{C} \equiv \frac{C}{\Gamma(1+\gamma)}. \tag{C.2}$$

Use the relation

$$\frac{k!}{\Gamma(1+\gamma k)} = \frac{\Gamma(1+k(1-\gamma))}{[\gamma^\gamma(1-\gamma)^{1-\gamma}]^k} \cdot \chi(k)$$

with the finite factor $\chi(k)$ from (2.11b), which decreases slowly above $k \sim 1$ (see Appendix B). We drop the factor χ for now and when it comes to finding the distribution $\Psi(\nu)$, we will recall and evaluate it at a characteristic point $k = k_{\text{sd}}(\nu)$.

C.1 Constructing the source function $\Psi(\nu)$

The moments take the form

$$g_k = 2\left(k+\frac{1}{3k}\right)\frac{\Gamma(1+k(1-\gamma))}{D^k}\chi(k). \tag{C.3a}$$

with $D(\gamma)$ defined by (2.10).

Observing that

$$k \cdot \Gamma(1+k(1-\gamma)) = \frac{([1+k(1-\gamma)]-1)\,\Gamma(1+k(1-\gamma))}{1-\gamma},$$

and

$$\frac{1}{k}\Gamma(1+k(1-\gamma)) = (1-\gamma)\Gamma(k(1-\gamma)),$$

we get a sum of Gamma-functions with shifted arguments:

$$g_k = \frac{2\mu}{D^k}\left[\Gamma(2+k\mu^{-1}) - \Gamma(1+k\mu^{-1}) + \frac{1}{3\mu^2}\Gamma(k\mu^{-1})\right]. \tag{C.3b}$$

Now we look for a function Ψ_τ ($\tau = 2, 1, 0$) whose Mellin moments reproduce

$$\Gamma(\tau + k\mu^{-1}) \cdot D^{-k}. \tag{C.4}$$

Taking Ψ_τ in the form

$$\Psi_\tau(x) = \psi_0 \cdot D(Dx)^{\epsilon_\tau} e^{-[Dx]^\mu}, \tag{C.5}$$

and introducing $z = (Dx)^\mu$ as integration variable,

$$\int_0^\infty dx\, x^k \Psi_\tau(x) = \psi_0 D^{-k} \int_0^\infty dy\, y^{k+\epsilon_\tau} e^{-y^\mu} = \frac{\psi_0}{\mu} D^{-k} \int_0^\infty dz\, z^{[k+\epsilon_\tau-(\mu-1)]/\mu} e^{-z}$$

$$= \left[\frac{\psi_0}{\mu}\right] \cdot \frac{\Gamma(k\mu^{-1} + (\epsilon_\tau + 1)\mu^{-1})}{D^k}. \tag{C.6}$$

Compared with (C.4) the result is as follows

$$\mu = \frac{1}{1-\gamma}, \tag{C.7a}$$

$$\psi_0 = \mu, \tag{C.7b}$$

$$\epsilon_\tau = \tau \cdot \mu - 1. \tag{C.7c}$$

Introducing the short notation

$$\kappa(x) \equiv [Dx]^\mu, \tag{C.8a}$$

the final answer for the multiplicity distribution in a gluon jet becomes

$$\Psi(\nu) = \frac{2\mu^2}{\nu}\left[\kappa^2(\nu) - \kappa(\nu) + \frac{1}{3\mu^2}\right]e^{-\kappa(\nu)} \cdot \chi(k_{\rm sd}). \tag{C.8b}$$

At the point $\gamma = 0$ (C.8) turns into the DLA answer.

C.2 $k_{\rm sd} = \mu(\kappa - 2)$

We determine the value of the characteristic moment $k_{\rm sd}(\nu)$ from the position of the Steepest Descent point of the integration over $\ln z$ in (C.6). Analysing the interplay between the exponential falloff and increase of the integrand driven by the leading power of κ, we deduce $k_{\rm sd} + \epsilon_2 + 1 = \mu z$:

$$k_{\rm sd}(\nu) = \mu\left([D\nu]^\mu - 2\right) = \mu\left(\kappa(\nu) - 2\right). \tag{C.8c}$$

This prescription is definitely valid for the tail of the distribution and works well as long as $\nu \gtrsim 1$.

The trouble continuing the tail $\Psi(\nu)$ down towards $\nu = \mathcal{O}(1)$ hits when

$$k_{\rm sd} = \mu\left([D\nu]^\mu - 2\right) = 0.$$

For a realistic value $\gamma \simeq 0.4$,

$$D \simeq 1.5, \quad \mu \simeq 5/3,$$

and $k_{\rm sd}(\nu)$ vanishes at $\nu \approx 1$. Below this point χ becomes complex, setting the limit of applicability of the tail formula (C.8b): see Fig. 22.
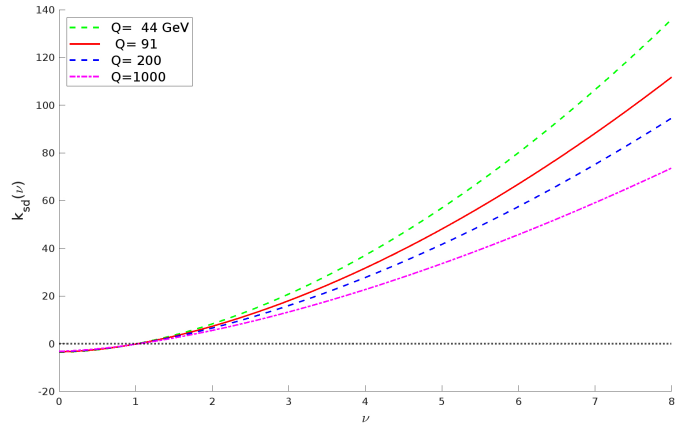

Figure 22: Variation of $k_{\rm sd}$ with ν

Equations (C.8) solve the quest.

C.3 An alternative approach to the ratio of Γ functions and $k_{\rm sd} = \mu(\kappa - \frac{3}{2})$

With the help of Nemes approximation (B.2a) it is straightforward to derive another relation that covers factorials, exponents **and** powers of k:

$$\left[\gamma^\gamma(1-\gamma)^{(1-\gamma)}\right]^k \cdot \frac{\Gamma(1+k)}{\Gamma(1+\gamma k)} = \Gamma(\tfrac{1}{2} + (1-\gamma)k) \cdot \mathcal{F}. \tag{C.9a}$$

Here $\mathcal{F}$ is a new slowly changing prefactor in place of χ (2.11b)

$$\mathcal{F}(k,\gamma) = \frac{1}{\sqrt{2\pi}}\sqrt{\frac{1+k}{1+\gamma k}} \cdot \frac{\mathcal{R}(1,k)}{\mathcal{R}(1,\gamma k)\mathcal{R}(\frac{1}{2},(1-\gamma)k)}, \tag{C.9b}$$

where

$$\mathcal{R}(\Delta, k) \equiv e^{-\Delta}\left(1 + \frac{\Delta}{k}\right)^k \cdot \left(1 + \frac{1}{12(\Delta+k)^2}\right)^{\Delta+k}. \tag{C.9c}$$

Then we invoke the DLA factor,

$$2\left(k + \frac{1}{3k}\right) \cdot \frac{\Gamma(1+k)}{\Gamma(1+\gamma k)},$$

and use machinery similar to that of (C.3).

Observing that

$$k \cdot \Gamma(\tfrac{1}{2} + k(1-\gamma)) = \frac{\left([\tfrac{1}{2} + k(1-\gamma)] - \tfrac{1}{2}\right)\Gamma(\tfrac{1}{2} + k(1-\gamma))}{1-\gamma} = \mu\left[\Gamma(\tfrac{3}{2} + k(1-\gamma)) - \tfrac{1}{2}\Gamma(\tfrac{1}{2} + k(1-\gamma))\right],$$

we get a sum of Gamma-functions with shifted arguments:

$$g_k = \frac{2\mu}{D^k}\left[\Gamma(\tfrac{3}{2} + k\mu^{-1}) - \left(\frac{1}{2} - \frac{1}{3\mu k}\right)\Gamma(\tfrac{1}{2} + k\mu^{-1})\right] \cdot \mathcal{F}. \tag{C.10}$$

We did not play with the last "1/3" correction term $\mathcal{O}(k^{-2})$ since the perspective of dealing with Γ of a negative argument did not look attractive. Anyway, its contribution is hardly noticeable.

This leads to an alternative form of the answer:

$$\Psi(\nu) = \frac{2\mu^2}{\nu}\left([D\nu]^{\frac{3}{2}\mu} - \frac{1}{2}[D\nu]^{\frac{1}{2}\mu} + \frac{1}{3\mu}[D\nu]^{-\frac{1}{2}\mu}\right) \cdot \mathcal{F}(k_{\text{sd}}). \tag{C.11}$$

This one may look less pretty than (C.8) but can come in handy. Here, the leading power of $\kappa = [D\nu]^{\mu}$ has decreased from 2 to $\tfrac{3}{2}$ because a $1/\sqrt{\kappa}$ factor coming from χ was taken into account to determine the optimal argument of the function Γ in (2.12). Correspondingly, the Steepest Descent point is shifted and the characteristic moment k_{sd} now has $\tfrac{3}{2}$ in place of the 2 in (C.8c).

The two expressions are formally identical asymptotically, $k \to \infty$. However, the difference between (C.8) and (C.11) exists and has a reason and a certain meaning. The point is, what values of ν are we interested in.

The key parameter that determines which of the two is better suited is the value of $\gamma \cdot k$. It is the very parameter that formed the basis for the MDLA approach.

In order to adequately determine the characteristic moment rank k_{sd} that is the core element of our back-and-forth exercise in the Laplace transformation, one needs the prefactor, χ or $\mathcal{F}$, to be roughly constant. Neither of them is precisely so, but their slow change with k, either when $k \to \infty$ (the case of χ) or in the origin ($\mathcal{F}$) is guaranteed to leave the height and shape of the tail unaffected.

factor	at $k = 0$	at $k \to \infty$
$\chi(k)$	$\dfrac{12}{13}\dfrac{e}{\sqrt{2\pi}}$	$\dfrac{1}{\sqrt{2\pi\gamma(1-\gamma)\cdot k}}$
$\mathcal{F}(k)$	$\sqrt{\dfrac{e}{2\pi}}$	$\dfrac{1}{\sqrt{\gamma}}$

C.4   Comparison

Fig. 23 demonstrates how the two alternative representations (2.13) compete in practice. The tails are indistinguishable. Meanwhile, the "$\tfrac{3}{2}$" version (2.13b) extends slightly further below $\nu = 1$ than its counterpart (2.13a). The vertical lines mark the domain of applicability of the respective formulae.

We make this note not because the temptation to peek down below 1 is legitimate within our approach but rather because it raises a question to be addressed in the future.

D   Running coupling

We employ the 2-loop coupling satisfying

$$\frac{d}{d\ln Q^2}\frac{\alpha_s(Q)}{4\pi} = -\beta_0\left(\frac{\alpha_s(Q)}{4\pi}\right)^2 - \beta_1\left(\frac{\alpha_s(Q)}{4\pi}\right)^3 \tag{D.1a}$$

with

$$\beta_0 = \frac{11}{3}N_c - \frac{2}{3}n_f = 11 - \frac{2}{3}n_f, \quad \beta_1 = \frac{34}{3}N_c^2 - 2C_F n_f - \frac{10}{3}N_c n_f = 102 - \frac{38}{3}n_f. \tag{D.1b}$$
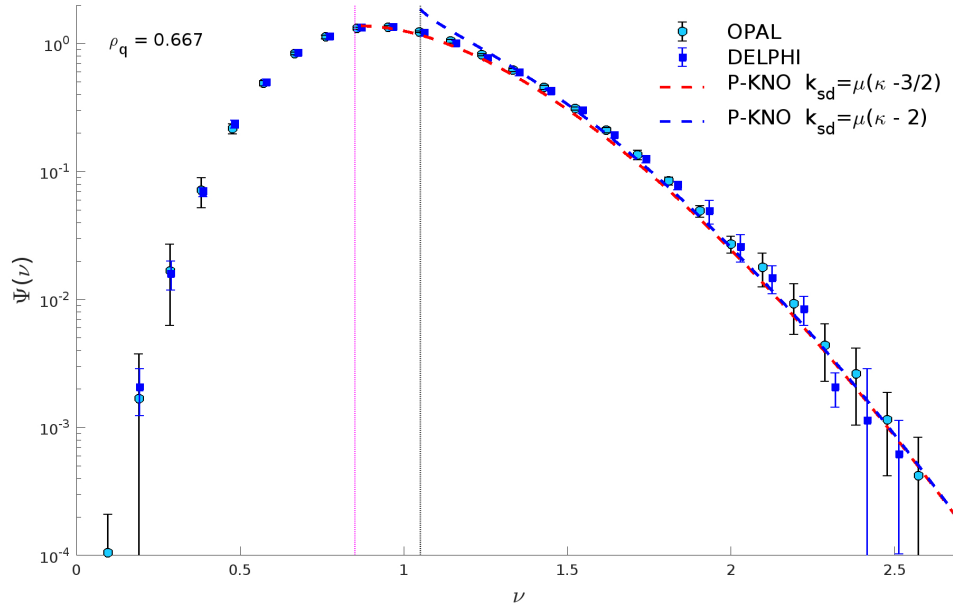
Figure 23: Comparison between two representations (2.13) of the P-KNO tail

This yields the differential equation

$$\frac{d}{d\ln Q}\left(\frac{2\pi}{\alpha_s(Q^2)}\right) = \beta_0 + \frac{1}{2}\beta_1\left(\frac{\alpha_s(Q)}{2\pi}\right) \tag{D.2}$$

with the approximate solution

$$\frac{\alpha_s(Q)}{2\pi} = \left(\beta_0 Y + \frac{\beta_1}{2}\ln Y + \text{const}\right)^{-1}, \tag{D.3}$$

where $Y = \ln(Q/\Lambda_{\text{QCD}})$. This form, where one keeps the term $\ln Y$ in the denominator without expanding in $\ln Y/Y$, is convenient in one respect: it allows one to easily relate the desired value of the coupling with the Λ_{QCD} parameter. For example, should we want $\alpha_s(M_Z)$ to be equal to a given value α_Z, we simply solve the equation

$$\alpha_Z = 2\pi\left(\beta_0\ln\frac{Q}{\Lambda_{\text{QCD}}} + \frac{\beta_1}{2}\left[\ln\ln\frac{Q}{\Lambda_{\text{QCD}}} - \ln\ln\frac{M_Z}{\Lambda_{\text{QCD}}}\right]\right)^{-1}, \tag{D.4a}$$

$$\Lambda_{\text{QCD}} = M_Z \cdot \exp\frac{2\pi}{\beta_0\alpha_Z}. \tag{D.4b}$$

By the way, both the second loop term and not expanding the denominator have a little impact on the results.

We remind the reader that since multiplicities are driven by soft-gluon radiation, we employ the *physical* coupling, also known as the "bremsstrahlung" or CMW [17], scheme.

E Constructing $\Psi^{(\rho)}$ in the general case $\rho \neq 1$

We represent Ψ as

$$\Psi(x) = \frac{1}{x}e^S, \qquad S = \ln(x\Psi(x)).$$

29

E.1 Laplace transform $\nu \to \beta$

Evaluate the Laplace transform:

$$\Phi(\beta) \quad = \quad \int_0^\infty \frac{dx}{x} \exp\left(S(x) - \beta x\right). \tag{E.1a}$$

The Steepest Descent in $\ln x$ gives

$$S_x(x_{sd}(\beta)) \quad = \quad \beta\, x_{sd}(\beta), \qquad S_x(x) \equiv \frac{dS(x)}{d\ln x}. \tag{E.1b}$$

(E.1b) determines x_{sd} as a function of β.

The second derivative of the exponent (E.1a) reads

$$S_{xx} - \beta x = S_{xx} - S_x, \tag{E.1c}$$

where we used (E.1b). The answer for the Laplace image of Ψ becomes

$$\Phi(\beta) \quad \simeq \quad \sqrt{\frac{2\pi}{S_x - S_{xx}}} \exp\left\{S(x_{sd}) - S_x(x_{sd})\right\}. \tag{E.1d}$$

E.2 Inverse Laplace transform $\beta \to \nu$

Now we construct the Laplace image of the P-KNO distribution for an ensemble with "relative strength" ρ as[4]

$$\Phi^{(\rho)}(\beta) = \left[\Phi\left(\frac{\beta}{\rho}\right)\right]^\rho. \tag{E.2}$$

Redefining the integration variable $\beta'/\rho \to \beta$

$$
\begin{aligned}
\Psi^{(\rho)}(\nu) \quad &= \quad \int \frac{d\beta'}{2\pi i} \exp\left(\beta'\nu + \rho \cdot [S - S_x]_{x_{sd}(\beta'/\rho)}\right) \cdot \left[\sqrt{\frac{2\pi}{S_x - S_{xx}}}\right]^\rho \\
&= \quad \rho \int \frac{d\beta}{2\pi i} \exp\left\{\rho\left(\beta\nu + [S - S_x]\big|_{x_{sd}(\beta)}\right)\right\} \cdot \left[\sqrt{\frac{2\pi}{S_x - S_{xx}}}\right]^\rho.
\end{aligned}
\tag{E.3}
$$

Now look for the stationary point in β:

$$\nu + \frac{d}{d\beta}[S - S_x] = \nu + \frac{d\ln x_{sd}(\beta)}{d\beta}[S_x - S_{xx}]. \tag{E.4}$$

Using the S.D. equation (E.1b) we derive

$$
\begin{aligned}
S_x(x_{sd}(\beta)) \quad &= \quad \beta x_{sd}(\beta) \\
\frac{d}{d\beta} S_x(x_{sd}(\beta)) = S_{xx}\frac{d\ln x_{sd}}{d\beta} \quad &= \quad \frac{d}{d\beta}[\beta x_{sd}(\beta)] = x_{sd} + \beta x_{sd}\frac{d\ln x_{sd}}{d\beta}
\end{aligned}
\tag{E.5}
$$

$$\frac{d\ln x_{sd}(\beta)}{d\beta} \quad = \quad \frac{x}{S_{xx} - \beta x_{sd}}. \tag{E.6}$$

Substituting into (E.4) leads to

$$\nu + \frac{d}{d\beta}[S - S_x] = \nu - \frac{S_{xx} - S_x}{S_{xx} - \beta x} \cdot x = 0, \tag{E.7}$$

Substituting (E.1b) one more time, we get an expected "comeback":

$$(E.7) \implies \frac{\nu}{x} = \frac{S_{xx} - S_x}{S_{xx} - \beta x_{sd}} = \frac{S_{xx} - S_x}{S_{xx} - S_x} = 1. \tag{E.8}$$

---

[4]In the book [9] the factor $1/\rho$ was missed from the argument of the function Φ of (E.2). This resulted in an erroneous statement about the tail of the distributions.

We also need the second derivative of the exponent of (E.3),

$$T \equiv \rho\left(\beta\nu + [S - S_x]\big|_{x_{sd}(\beta)}\right) :$$

$$T_{\beta\beta} = \rho\frac{d}{d\beta}\left\{\nu - \frac{S_{xx} - S_x}{S_{xx} - \beta x}\cdot x\right\} = \rho\frac{d}{d\beta}\{\nu - x\} = -x\rho\frac{d\ln x_{sd}(\beta)}{d\beta} = -\rho\frac{x^2}{S_{xx} - S_x} \tag{E.9}$$

Making use again of

$$\beta\nu = \beta x \cdot \frac{\nu}{x} \overset{(E.1b)}{=} S_x \cdot \frac{\nu}{x} \overset{(E.8)}{=} S_x \cdot 1,$$

one finally arrives at

$$T = \rho\big(\beta\nu + [S - S_x]\big) = \rho\cdot S. \tag{E.10}$$

E.3 Assembling the pieces

Assembling the Gaussian factors we arrive at

$$\Psi^{(\rho)}(\nu) = \frac{\rho}{2\pi}\sqrt{\frac{2\pi}{T_{\beta\beta}}}\left[\sqrt{\frac{2\pi}{S_x - S_{xx}}}\right]^\rho \cdot e^T \overset{(E.9)}{=} \sqrt{\rho}\,\frac{\left[\nu\Psi(\nu)\right]^\rho}{\nu}\cdot\left[\frac{2\pi}{S_x - S_{xx}}\right]^{(\rho-1)/2} \tag{E.11}$$

Up to now our manipulations were general.

Now we invoke the structure of $\Psi(\nu)$ to derive

$$S = -\kappa + 2\ln\kappa + \mathcal{O}(\kappa^{-1}), \quad S_x = -\mu\kappa\left(1 - \frac{2}{\kappa}\right), \quad S_{xx} = -\mu^2\kappa,$$

$$S_x - S_{xx} = \mu(\mu-1)\kappa + 2\mu = \gamma\mu^2\kappa + 2\mu = \mu^2(\gamma\kappa + 2(1-\gamma)). \tag{E.12}$$

Invoking Ψ from (C.8) the answer take the final form

$$\Psi^{(\rho)}(\nu) = \frac{\sqrt{\rho}\mu}{\nu}\left(2\mu\left[\kappa^2 - \kappa + \frac{1}{3\mu^2}\right]\chi(\mu\kappa)\right)^\rho\cdot e^{-\rho\kappa}\cdot\left(\frac{2\pi}{\gamma\kappa + 2(1-\gamma)}\right)^{(\rho-1)/2}, \qquad \kappa = [D\nu]^\mu. \tag{E.13}$$

For realistic values of $\gamma \sim 0.4$, we have $\kappa \sim (1.5\nu)^{1.7}$ and the sum in square brackets in the pre-exponent of Ψ is positively definite for $\nu > 0.6$, so no problem for $\nu \gtrsim 1$.

The alternative version (C.11) permits us to descend a little below $\nu = 1$ before failing.

E.4 Analysis of the β plane

Returning to the Laplace image, let us discuss a few interesting points.

Since $\Psi(x)$ falls with $x \to +\infty$ faster than exponentially, the resulting image is regular at any finite β in the complex plane. This means that $\Phi(\beta)$ has an essential singularity at $\beta = \infty$.

It is straightforward to see by examining the S.D. equation

$$-\beta x - \mu(Dx)^\mu + 2\mu = 0 \tag{E.14a}$$

which determines indirectly the dependence of the S.D. point x_{sd} on β as

$$\mu\frac{[Dx]^\mu - 2}{x} = -\beta, \qquad x = x_{sd}(\beta). \tag{E.14b}$$

In general, this relation cannot be solved analytically. Meanwhile, by taking x_{sd} large, one can solve it approximately:

$$\mu[Dx]^{\mu-1} \approx -D\beta, \qquad \kappa \equiv [Dx]^\mu = \left(-\mu^{-1}D\beta\right)^{\mu/(\mu-1)} \propto \left(-\beta\right)^{1/\gamma}.$$

This exercise demonstrates that the function is multi-valued. When exponentiated, it leads to oscillations at infinity which become wild when the coupling decreases to zero.

In this way a regular function tries to mimic a pole that has to be there in the DLA limit $\gamma = 0$.

E.4.1 Explicit expression for $\Phi(\beta)$

To see whether our solution reproduces the transition to DLA, and how well it does it, we first have to write down Φ explicitly.

We have derived above

$$\Phi(\beta) \simeq \sqrt{\frac{2\pi}{S_x - S_{xx}}} \exp\left\{S(x_{sd}) - S_x(x_{sd})\right\} \qquad (E.15)$$

with

$$S(x) = \ln(x\,\Psi(x)).$$

Having invoked the function Ψ from (C.8), we obtained above

$$S_x = -\mu(\kappa - 2) \qquad (E.16)$$
$$S_{xx} = -\mu^2\kappa \qquad (E.17)$$
$$S_x - S_{xx} = \mu^2(\gamma\kappa + 2(1-\gamma)) \qquad (E.18)$$

where in the pre-exponent we kept the leading second power of κ only.

Now,

$$\sqrt{\frac{2\pi}{S_x - S_{xx}}} = \frac{\sqrt{2\pi}}{\mu\sqrt{\gamma\kappa + 2(1-\gamma)}}$$

and (E.15) becomes

$$\Phi(\beta) = \frac{\sqrt{2\pi}\mu}{\sqrt{\gamma\kappa + 2(1-\gamma)}} \cdot 2\left[\kappa^2 - \kappa + \frac{1}{3\mu^2}\right] \cdot e^{(\mu-1)\kappa - 2\mu}\chi(k_{\rm sd}), \qquad \kappa \equiv \kappa(x_{sd}(\beta)). \qquad (E.19)$$

$$S_x(x_{sd}(\beta)) = \beta\, x_{sd}(\beta), \qquad S_x(x) \equiv \frac{dS(x)}{d\ln x}. \qquad (E.20)$$

E.4.2 DLA

At $\gamma = 0$ (E.14b) turns into

$$\frac{Cx - 2}{x} = -\beta \implies x_{sd} = \frac{2}{C + \beta}. \qquad (E.21)$$

Substituting in (E.19) we recover the second-order DLA pole almost perfectly normalized:

$$\Phi^{[DLA]}(\beta) \simeq \sqrt{2\pi} \cdot 2\left[\left(\frac{2C}{C+\beta}\right)^2 + \dots\right]e^{-2}\chi(0) = \frac{2C^2}{(C+\beta)^2} \times \frac{4\sqrt{\pi}}{e^2}, \qquad (E.22)$$

$$\frac{4\sqrt{\pi}}{e^2} \approx 0.96 \qquad \text{in place of 1}. \qquad (E.23)$$

F Playing with a toy model

F.1 Multiplicity and correlations in RSE

Since we have a toy, let's play. Let us estimate in a more quantitative manner what snake-tongue configurations, RSE, bring into the game.

The first thing to notice is an intricate balance of the hardness scales of the two leading subjets. As we saw above, a more energetic parton wins a broader cone to harvest from ([27]). So, the hardness scales become

$$Q_g = z_g 2Q, \quad Q_q = z_q 2Q = (1 - z_g)2Q. \qquad (F.1)$$

Here Q represents the full hardness of the CMS jet, $Q = 2 * 550\,\text{GeV} * \sin(R/2) = 430\,\text{GeV}$ resulting in $\gamma = 0.38$.

A rough qualitative estimate of the total RSE multiplicity is as follows:

$$\langle N_{\text{RSE}}(Q)\rangle = N_q\big((1 - z_g)^2 Q\big) + N_g\big(z_g^2 Q\big) \simeq \big[(1 - z_g)^{2\gamma} + \rho_q^{-1} z_g^{2\gamma}\big] \cdot N_q(Q). \tag{F.2}$$

The snake multiplicity relative to a single-quark jet increases steadily with z_g until it reaches its maximum value 1.56 at very large $z_g \simeq 0.85$. At $z_g = \frac{1}{3}$ as in Fig. 17 the multiplicity gain is also not small: a factor of 1.39.

The excess multiplicity yield is welcome: It is what the rattlesnakes were called for.

A simple analysis of inclusive measurement of two particles allows splitting the second factorial multiplicity moment into two parts,

$$\langle N_{\text{RSE}}(N_{\text{RSE}} - 1)\rangle = \Big[\langle N_{\text{RSE}}(N_{\text{RSE}} - 1)\rangle - 2N_q N_g\Big]\Big|_{same} + \Big[2N_q N_g\Big]\Big|_{away}. \tag{F.3}$$

The away-side correlation is maximal,

$$2N_q N_g = \frac{1}{2}\langle N_{\text{RSE}}\rangle^2, \tag{F.4}$$

at $z_g \simeq 0.38$, not far from our ad hoc model configuration.

F.2 Moving the tongue

Now we can release the stringent prescription dictated by the kinematics of Fig. 17 in order to see how the RSE evolves.

In our discussion of the ATLAS tail, we examined how the energy sharing and angle of the hard split tongue vary with the normalized event multiplicity ν. Combining (4.7) for the angular push with (4.8), which provided an elementary estimate of the angle of tongue split, we can characterise the typical transverse momentum, j_t in CMS notation, in the RSE at a given ν. A bold estimate (which includes taking the mean value as the exponential of the mean logarithm) looks as follows:

$$\frac{j_t^{(tongue)}}{Q} = \Big\langle z_g \Big\rangle \cdot \Big\langle \frac{\theta_1}{R} \Big\rangle \sim z_{typ}(q) \cdot \exp\Big(-\frac{1}{q\gamma}\Big). \tag{F.5}$$

Here z_{typ} is given by

$$\Big\langle \ln \frac{1}{z_{typ}} \Big\rangle \simeq \psi\big(1 + q\gamma\big) - \psi\big(\tfrac{1}{2}q\gamma\big),$$

and for q we substitute the characteristic momentum rank defined in (4.11),

$$q = q_{char}(\nu) = \mu\Big(\rho\big([D\nu]^{2\mu} - \tfrac{3}{2}\big) + \tfrac{1}{2}\Big), \qquad \mu = \frac{1}{1 - \gamma}.$$

The momentum fraction share is pushed up rather fast with increasing multiplicity. The opening angle of the tongue is more inert in its approach to R. The result for the CMS environment ($E_{jet} = 550\,\text{GeV}, R = 0.8, Q = 430\,\text{GeV}$) is shown in Fig. 24.

To produce Fig. 24, we used a more careful estimate of the pseudorapidity distance $\delta\eta^*$ between the RSE gluon and the cone border:

$$\langle \delta\eta^* \rangle = \frac{1}{q\gamma}\left[1 - \frac{q\gamma\Delta_\eta}{\exp(g\gamma\Delta_\eta) - 1}\right]. \tag{F.6}$$

Here Δ_η is the maximum rapidity span available to QCD radiation,

$$\Delta_\eta = \ln\frac{Q}{Q_0}.$$

where Q_0 is the hadron scale that sets limit on collinear QCD radiation. We do not need to specify it here because the angular squeeze in the domain shown in Fig. 24 is totally insensitive to it.

When the parameter $q\gamma$ is small, the radiation is not restricted and (F.6) produces $\langle \delta\eta^* \rangle = \frac{1}{2}\Delta_\eta$. It becomes squeezed, $1/q\gamma$, when $q\gamma \gg 1$.

With $\nu \to \infty$, the "average angle" normalized to R and "energy fraction" of the RSE saturate at 1 and 0.5, respectively. The "hardness" j_t tends to $\frac{1}{2}Q$, which is the correct limit: In the rest frame of their virtual parent, the two partons fly apart at a $90°$ angle with equal energies $j_t = \frac{1}{2}Q$.
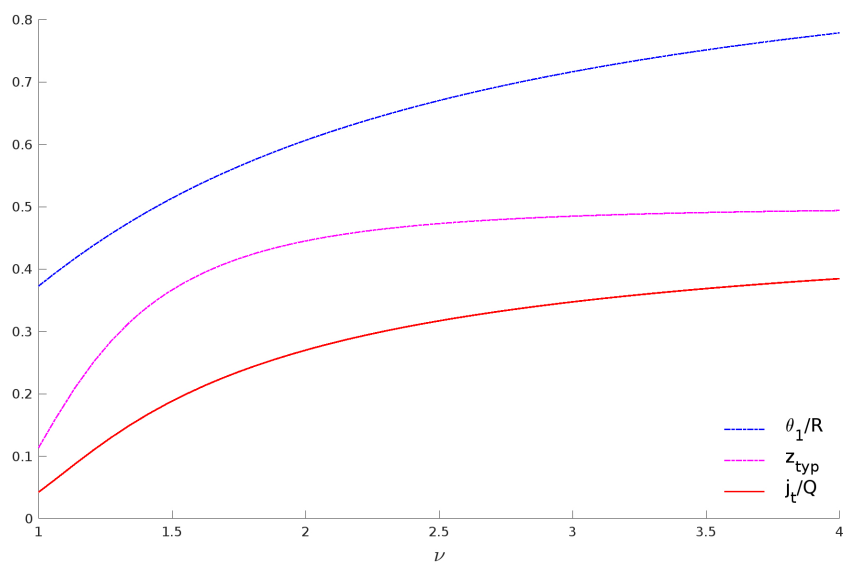
Figure 24:   Characteristics of typical RSE configurations